Master's thesis

NTNU
Norwegian University of Science and Technology
Faculty of Natural Sciences
Department of Physics

Elisabeth Rolandsgard Kjellevold

Stratospheric ozone depletion after very large solar proton events

Master's thesis in Physics
Supervisor: Patrick J. Espy
Co-supervisor: Jia Jia
February 2024

NTNU
Norwegian University of
Science and Technology

Elisabeth Rolandsgard Kjellevold

Stratospheric ozone depletion after very large solar proton events

Master's thesis in Physics
Supervisor: Patrick J. Espy
Co-supervisor: Jia Jia
February 2024

Norwegian University of Science and Technology
Faculty of Natural Sciences
Department of Physics

NTNU
Norwegian University of
Science and Technology

Aknowledgements

First and foremost, I want to give thanks to God, for creating this wonderful planet, and for giving me the opportunity to study it. It has been a bumpy road, but He has given me strength and joy every step of the way.

Many thanks to my supervisors Prof. Patrick Espy, Dr.Jia Jia and Dr.Yvan Orsolini. The meetings with you have been an invaluable source of ideas, and given the project direction. I am deeply grateful for all patience, helpful feedback and encouragements. And special thanks to Jia for her help with model problems and for providing the necessary data. Thanks should also go to Donal Murtagh for letting me use his model.

I also want to thank my friends, you have made my time here in Trondheim truly joyful. Thank you for all good times, all laughs and all coffee breaks. Lastly, to Daniel, my amazing husband, for all love and support. This would not have been possible without you.

Abstract

The energetic particles from Solar Proton Events(SPEs), predominantly protons, can penetrate into the middle atmosphere, initiating complex ion chemistry processes that lead to the formation of odd hydrogen (HO_x) and odd nitrogen (NO_x). These chemical species, particularly NO_x, play a significant role in catalytic ozone destruction.

Historical satellite observations and modeling studies have provided evidence of increased NO_y levels and ozone depletion following large SPEs. However, the impact of extreme and rare SPEs on ozone depletion relies heavily on model predictions. This study aimed to explore the chemical impacts of SPEs on stratospheric ozone using a comprehensive chemical box model(MISU-1D), and hence provide a parameteration for ozone loss with given EPP-NOy.

Specifically, at 40 km altitude and 70°N, simulations demonstrated nearly complete ozone destruction at night under extreme NO_y conditions(800ppbv), with an ozone loss of about 80 percent persisting throughout the day. There was no clear saturation point observed, indicating that increasing NO_y levels continue to impact ozone levels.

The study also highlighted the importance of photolysis in ozone depletion, with the lack of photolysis leading to negligible ozone loss in nighttime simulations. Ozone destruction was more effective at 80N than at 70N in late October. At 80N, the photolysis of NO_2 enable catalytic ozone destruction, meanwhile the lack of shortwave radiation hinders ozone production. MISU-1D agreed within 10 percent with results simulated by SD-WACCM-D.

Sammendrag

Energiske partikler fra solstormer (Solar Proton Events; SPE), hovedsakelig protoner, kan starte komplekse ion-prosesser som produserer odd-nitrogen(NO_x) og odd-hydrogen(HO_x) i mesosfæren og stratosfæren. Disse molekylene kan ødelegge ozon via katalytiske reaksjoner. Spesielt produksjon av av NO_x spiller en betydelig rolle for ozon i stratosfæren på grunn av sin lange levetid.

Satellittobservasjoner og modelleringsstudier viser forhøyede verdier av NO_y, og lavere verdier av O_3 etter store solstormer. Derimot er virkningene av ekstremt store solstormer avhengig av modellprognoser. Denne studien hadde som mål å undersøke konsekvensene av solstormer, og dermed forhøyede verdier av NO_y, på stratosfærisk ozon, ved å benytte en kjemisk boksmodell(MISU-1D). Denne sammenhengen kan bidra til en parameterisering for ozonnedbrytning gitt en viss mengde NO_y produsert av energiske partikler(EPP).

Ved 40 km og 70N viste simuleringene en nesten fullstendig ozon-kollaps om natten under ekstreme NO_y-forhold(800ppbv), med betydelig ozontap på omtrent 80 prosent som vedvarte hele dagen. Det ble ikke observert et klart metningspunkt for NO_y, som betyr at en videre økning kan fortsette å påvirke ozonnivåene.

Studien påpekte også betydningen av fotolyse i ozonnedbrytning, der mangel på fotolyse førte til ubetydelig ozontap i nattlige simuleringer. Ozonødeleggelsen var mer effektiv ved 80N enn ved 70N. Ved 80N muliggjorde fotolyse av NO_2 katalytisk ozonødeleggelse, samtidig som mangel på kortbølget stråling hindret ozonproduksjon. MISU-1D samsvarte bra med resultat simulert av SD-WACCM-D, med forskjeller i relativt ozontap på omtrent 10 prosent.

Contents

1 Introduction

Occasionally, the terrestrial atmosphere is bombarded by a substantial flux of charged particles. These particles originates from intense solar flares or coronal mass ejections, and the particles may be further accelerated by shocks as they travel through interplanetary space. This magnetic bubble of particles interacts with earths magnetic field, and is guided towards the polar caps. These events are referred to as Solar Proton Events (SPEs) and tend to occur during the high phase of the approximately 11-year solar cycle.

Apart from their captivating display of auroras and disruptive effects on power grids and telecommunication, SPEs may have a significant impact on atmospheric chemistry. The incoming energetic particles, predominantly protons, may have sufficient energy to penetrate into the middle atmosphere. Subsequently, through a cascade of complex ion chemistry, odd hydrogen (HO_x= H + OH + HO_2) and odd nitrogen (NO_x=N + NO + NO_2) is formed. NO_x has a nocturnal lifetime of days to weeks in the stratosphere, allowing it to react with ozone through the following catalytic cycle

$$\begin{aligned} &\mathrm{NO} + \mathrm{O_3} \longrightarrow \mathrm{NO_2} + \mathrm{O_2} \\ &\mathrm{NO_2} + \mathrm{O} \longrightarrow \mathrm{NO} + \mathrm{O_2} \\ &\text{net: } \mathrm{O} + \mathrm{O_3} \longrightarrow 2\,\mathrm{O_2}, \end{aligned}$$

resulting in a destruction of odd oxygen(O_x=O + O_3).

There has been several satellite observations of increases in NO_y and decreases in ozone in the aftermath of large SPEs(Jackman et al. 2001[1], Jackman et al. 2008[2]), along with several modelling studies with similar results(Jackman et al. 2008, Rodger et al. 2008[3], Calisto et al. 2012[4]). At the end of October 2003, there was a massive solar storm, coined *The Halloween Storms*. The following days portrayed an increase in NO_x by about 100 percent accompanied by up to a 30 percent decrease in ozone in the upper stratosphere(Rohen et al., 2005, Jackman et al., 2008)[5][2]. Figure 1 displays this event as simulated by the version of the Whole Atmospheric Community Climate Model with ion-chemistry of the D-region, and with Specified Dynamics(SD-WACCM-D)(Andersson et al., 2016)[6]. The plot shows the immediate direct ozone depletion in the mesosphere due to the short-lived HO_x increases, along with the long term stratospheric depletion caused by the descending tongue of NO_y.

Both the middle atmosphere's thermal structure and the circulation patterns are sensitive to stratospheric ozone, and a better understanding of the effects of SPEs on the stratosphere may improve climate models and operational prediction models. Additionally, and perhaps more importantly, the ozone layer protects life on Earth from hazardous UV radiation. If moderate-sized SPEs cause ozone depletion, could a great event be a serious threat to the ozone layer? The most intense SPE recorded

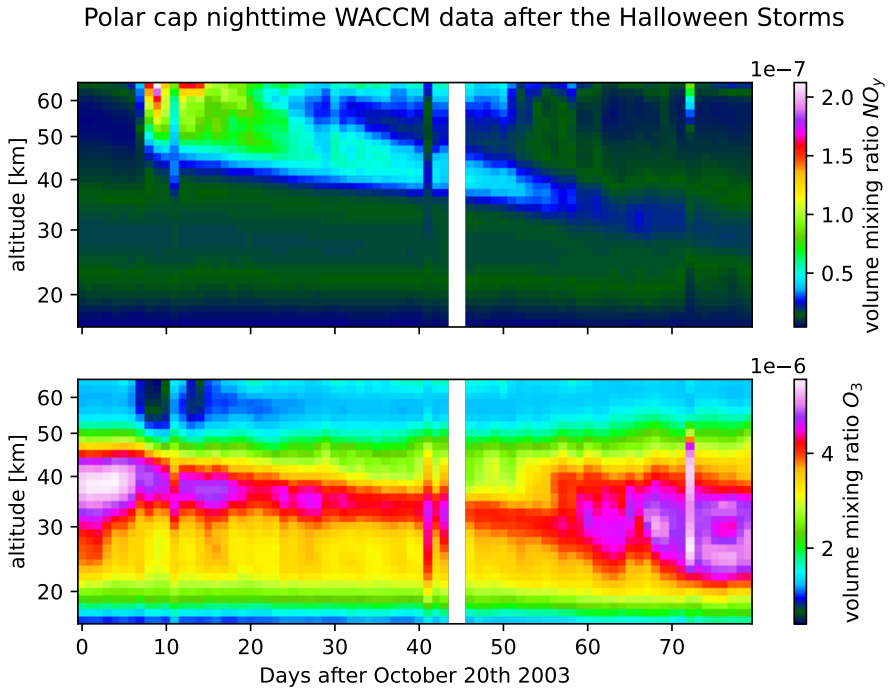

Figure 1: Shows the volume mixing ratio of NO_y(upper plot) and O_3(lower plot) in the aftermath of the Halloween storms in 2003. The data is simulated by SD-WACCM-D, and daily(nightly) polar cap values are sampled to fit with MIPAS observations of the same event.

within the past 11 millennia took place in 774-775 AD and serves as a worst-case scenario. This event was simulated in a 3D-chemistry-climate model by Sukhodolov et al. in 2017[7], aiming to replicate the elevated 10Be values found in ice cores. Reddmann et al.(2023)[8] simulated the same event, but chose an onset time in January with dynamics that maximize vertical coupling to simulate a true worst-case scenario. The most dramatic change was found in the following antarctic winter, with an ozone decrease of up to 80 percent at 30-35 km. One year later, a 20 percent ozone loss persisted in the northern stratosphere. Although these findings are drastic, it does not point toward a total collapse of the ozone layer, and the rareness of such events must be highlighted.

Although it seems like larger NO_x increases lead to greater ozone loss, the dependence does not seem to be linear, as the simulation of this event indicates. Rather, it seems like the ozone loss is saturated at some point, where adding more NO_x to the stratosphere will not decrease the ozone level further. This thesis aims to explore how the enhancement of NO_x after large SPEs affects the ozone in the polar stratosphere, and whether the associated ozone loss saturates at some amount of NO_x. A photo-chemical, one-dimensional model developed by Donal Murtagh(private communication), referred to as MISU-1D, will be employed. The question of ozone depletion will be studied for different altitudes, latitudes, and seasons of the SPE-onset, and the causes behind the loss will also be discussed.

This master thesis has 5 sections, including the introduction. First, the theory sec-

tion explores the physics of the atmosphere, and the chemistry of the stratosphere, before diving into the nature of a Solar Proton Event and its atmospheric impact. Then follows an overview of 3 models with increasing levels of complexity: a simple nighttime model, MISU-1D, and SD-WACCM-D. In section 4, the results generated by MISU-1D will be presented, discussed, and compared by the earlier simulations of Kalakoski et al.(2023)[9] with SD-WACCM-D. Finally, the conclusions of the work are presented in section 5.

2 Theory

2.1 The atmosphere

The atmosphere is defined as the envelope of gas surrounding a planet, and ours is kept in place by Earths gravity. Shielding us from hazardous radiation, providing pressure for water to remain liquid at the surface, and keeping the Earth warm via greenhouse gases, the terrestrial atmosphere is essential for life as we know it to thrive. However, the atmosphere may be perturbed by a range of factors, including natural phenomena such as the oxygen production of forests, the injection of pyroclasts into the troposphere during volcanic eruptions, and variations in space weather and solar irradiance. The last 50 years, anthropological pollution has been under scrutiny of the scientific community, as even minor species, as carbon-dioxide, methane and ozone, plays a vital role in the energy budget.

This subsection is based on Andrews(2010) [10], and aims to review the main features of the four atmospheric layers: the troposphere, the stratosphere, the mesosphere and the thermosphere. The most prominent circulation patterns of the middle atmosphere are also presented.

2.1.1 Vertical structure

The pressure profile of the atmosphere is established through a hydrostatic balance between the pressure gradient and the weight of the air masses above a parcel of air. Below 100 km, the pressure profile may be, to first order, estimated by the exponential decay

$$p = p_0 * \exp -h/H, \tag{1}$$

where $H = R * T_0/g$ is the scale height of an isothermal atmosphere of average temperature T_0. $R*$ is the specific gas constant. Since the air may be considered an ideal gas, it obeys

$$p = \rho R * T, \tag{2}$$

and thus the density ρ also follows this approximate exponential decay. This tendency for lower layers to have higher density is called density stratification. If a portion of air, called a parcel, is displaced vertically from its equilibrium, in most of the atmosphere, the buoyancy will act as a restoring force, moving it back towards its original position. Hence, the atmosphere is said to be stably stratified(Andrews, 2010).

The real atmosphere exhibits a temperature gradient, called the lapse rate, which vary with altitude. In fact, a sign reversal of the lapse rate is what marks the transition between the atmospheric layers. Figure 2 shows an idealized vertical profile of the temperature and the four layers: the troposphere, the stratosphere, the mesosphere and the thermosphere. Each of them is associated with a relatively

constant lapse rate, and with a pause where the lapse rate is zero. This structure is not constant, and the temperature, and even the altitude of the layers depend on latitude and season.

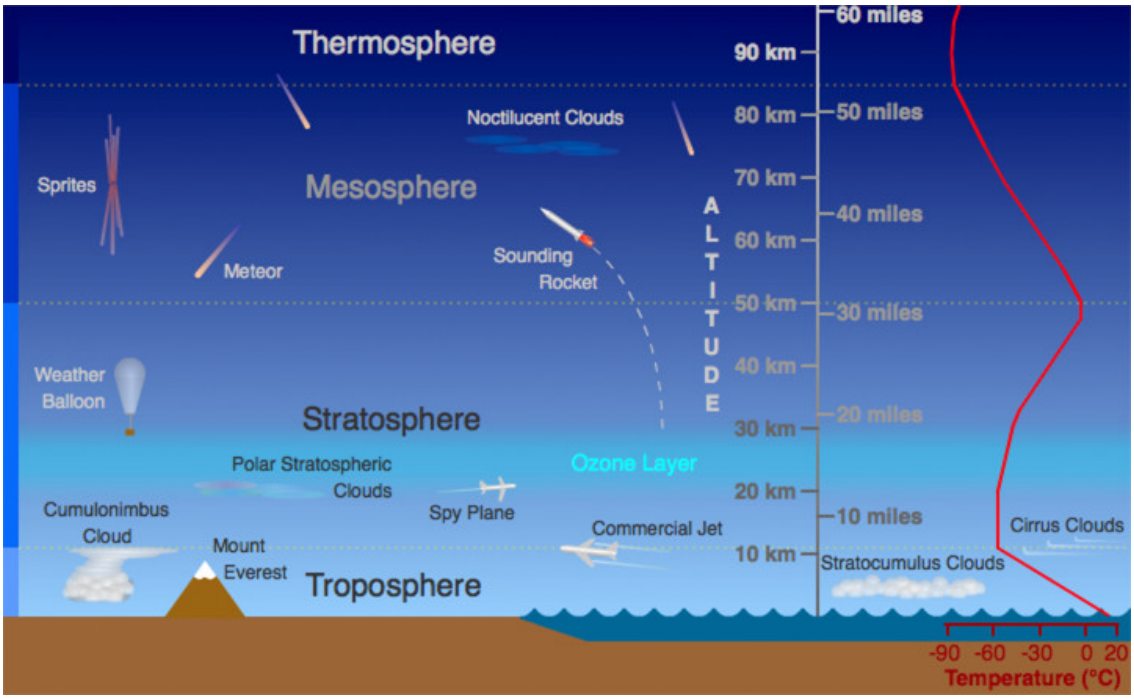

Figure 2: Shows the 5 atmospheric layers along with a course temperature gradient. Created by Randy Russel (UCAR).

The troposphere is the bottom layer of the atmosphere. Containing about 99 percent of all water vapour, this layer hosts most of the weather phenomena, like hurricanes, lightning and cloud formation. It is dominated by heating from the ground, resulting in a strong negative temperature gradient. Convection cells are formed by humid air that rises from the surface, before it cools and descends. This motion causes the troposphere to exhibit rapid vertical mixing. The temperature gradient changes sign at the tropopause, a region with lapse rate around zero displaying characteristics from both the troposphere and the stratosphere. This pause is found at about 7-8 km in the polar region, but as high as 14-18.5 km in the tropics, as the stronger convection cells transports the heat to higher altitudes. This tropical tropopause is known as the 'cold trap' due to its temperatures down to 200 K. The water vapour of the air masses moving through it will therefore freeze-dry and descend, leading to a very dry stratosphere. As the water-exchange between the troposphere and stratosphere is very small, the only chemical source of water in the stratosphere is photolysis of methane.

The word stratosphere literally means "sphere of layers". It is especially stably stratified, meaning the restoring buoyancy force moving vertically displaced parcels back to its equilibrium is very strong. This causes the layered structure, with little turbulence and vertical mixing. Moving upwards from the tropopause, the amount of ozone increases, reaching its maximum in number density around 23 km, and its maximum in volume mixing ratio around 36 km. The stratosphere contains about

90 percent of the atmospheric ozone, and heating due to UV-photolysis of ozone explains the positive lapse rate of this layer. The stratopause is located around 50 km. Above, in the mesosphere, the decreasing ozone concentrations lead to a negative lapse rate. In fact, the coldest temperatures in the atmosphere is found at the summer pole in the upper mesosphere, where the temperature may drop below 130K. Aside from the absence of ozone heating, this is due to radiative cooling by CO_2, enhanced by upwelling of air in the summer.

The mesosphere means "the middle sphere", a suiting name for several reasons. Being in the middle of the zones for conventional observation techniques, it is a hard region to study. Stretching between about 50km and 80km, it is out of reach for aircrafts and weather balloons, and yet its high atmospheric drag prevents satellites from orbiting. Furthermore, the mesosphere forms the middle atmosphere in union with the stratosphere. The mesopause serves as a separating region for two atmospheric properties; vertical mixing and ionization. Due to the negative lapse rate, the air in the mesosphere is more turbulent than in the stratosphere, and the air remains well-mixed up to around 105 km. At this altitude, the turbopause separates the homosphere below, from the heterosphere above. In the heterosphere, chemical species tend to organize in layers, determined by their molar masses. The upper mesosphere is partly ionized during the sunlit day, although with a high recombination rate. Due to this ionization, the upper mesosphere is sometimes considered as a part of the ionospheric D-layer. However, above the mesopause, in the thermosphere, ionization becomes an important feature, although ions are still a minor species. Due to the low density, the air becomes so rarefied that it can no longer be treated as a continuous fluid, but rather as a low-density plasma. The increasing dissociation of nitrogen and oxygen in the thermosphere heats the gas, resulting in a positive lapse rate. The thermosphere partly overlaps with the E and F region of the ionosphere, and is often said to end at about 500 km. The E-layer, ranging from about 90 km to 150 km, is ionized due to soft X-rays and far-UV solar radiation. The F-region extends outwards to about 500 km, but the distance is highly dependent on solar forcing. This region has a high electron density, and in contrast to the D and E region, it remains ionized during night. It is hard to draw an exact line of were the atmosphere ends, and space begins. However, the Kármán line draws the boundary at 100 km, as much for reasons of space regulations as for reasons of physics. On the night side of the Earth, particles bound by Earths gravity may wander as far out as 640 000 km, twice the distance to the moon(Baliukin et al., 2019)[11].

2.1.2 Circulation patterns

There are several physical laws governing the circulation of Earth atmosphere: conservation of energy, conservation of mass, and Newtons 2nd law of motion, also known as the momentum equation. For a parcel of air in a rotating frame of reference, the momentum equation is given by:

$$\frac{d\vec{v}}{dt} + \frac{1}{\rho}\vec{\nabla}p = 2\vec{\Omega}x\vec{v} + \vec{g} + \vec{F}, \tag{3}$$

where $\vec{v}$ is the velocity, $\vec{\Omega}$ is Earths angular velocity, $\vec{g}$ is the gravitational forces and $\vec{F}$ is the frictional forces. The pressure gradient $Vec\nabla p$ relates to the temperature gradient via the ideal gas law. As low latitudes receives more radiation than high latitude, this results in a meridional(north-south) pressure gradient. Sufficiently high up, the surface friction may be neglected, and the only force of comparable magnitude in 3 is the second term, the Coriolis force. This force acts perpendicular to the motion, and a balance may be obtained by a zonal wind, known as a geostrophic flow. Consequently, most transport occur in the zonal direction in Earths atmosphere, as the Coriolis force acts as a barrier against meridional flow, and vertical displacements are strongly inhibited by density stratification. However, there are large-scale atmospheric motions produced within these constraints, causing vertical and meridional mass exchange.

In the stratosphere, the most important dynamical pattern is called the Brewer-Dobson circulation (shown in figure 3), named after the two scientist that first suggested the physical model. In 1929 Dobson et al.[12] proposed a stratospheric meridional flow to reconcile the high ozone concentrations in the Arctic spring with the hypothesis that ozone is formed by action of sunlight. The same patterns were proposed by Brewer et al.[13] in 1949, as he sought an explanation for the dryness of the stratosphere. Knowing that the mixing ratio of helium was fairly constant up to 20 km, there had to be some mixing between the troposphere and the stratosphere. They concluded that the observations was best explained if " air circulates by a slow mean motion into the stratosphere at the equator, moves poleward in the stratosphere and sinks into the troposphere in temperate and polar regions". This hypothesis both explained how tropospheric air could be freeze-dried before entering the stratosphere, as well as supporting Dobsons explanation for ozone transport. The presence of a such a circulation was confirmed in the 1960s by following the movement of radioactive debris and volcanic aerosols(Butchart et al., 2014)[14], and a theoretical consistent dynamical model was provided by Dunkerton in 1978[15]. This model also included the mesospheric circulation.

The solstitial mesospheric circulation consists of upwelling of air at the summer pole, followed by transport towards the winter poles, where the air descends. The summer pole stratosphere is influenced by two different circulations: descending air below, and ascending air above. As a result, much of the stratosphere remains relatively motionless in the vertical direction. In the winter hemisphere however, these two circulation patterns work together, to form a strong downwelling in the polar region. The exact mechanisms behind the middle atmospheric circulations are not fully understood(Butchart et al. 2014)[14], but are thought to be driven by the dissipation of upward-propagating waves; the mesospheric circulation by gravity waves, and the Brewer-Dobson circulation by Rossby-waves(Andrews,2010)[10].

The stratospheric meridional flow encounters several obstacles in its path. Numerous tracers see a sudden drop of concentration at about 30 degrees, providing evidence for a fairly isolated tropical stratosphere, sometimes called the 'tropical pipeline'. This barrier is not stable, and eventually tongues of air stretches into the the mid-latitudes and mixes irreversibly. The timescale for airmasses to move from

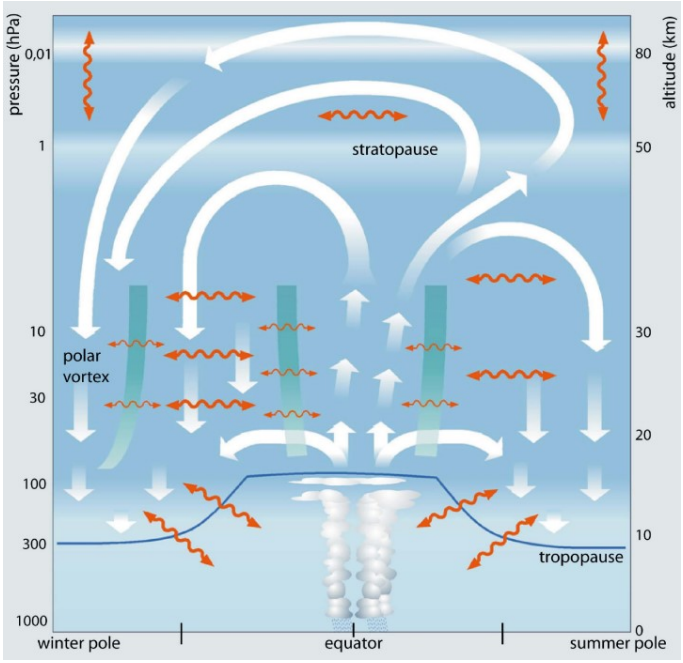

Figure 3: Schematic of the Brewer-Dobson circulation. The white arrows represent the mass streamfunction, and the wavy orange lines depict a two-way mixing. The thick green lines show stratospheric transport and mixing barriers. The figure is taken from by Bonisch et al (2011)[16], and was originally created by Ulrich Schmidt.

the tropics to the mid-latitudes is about a half to one year(Brasseur et al. 2005)[17]. Another significant barrier is the polar vortex, a band of strong westerly winds positioned around 60 degrees. It extends from about 16 km and upwards, isolating the polar regions. The main interaction between polar air and mid-latitude air is facilitated by large-scale Rossby waves, which pull off thin filaments of air along the vortex edge, and irreversibly mixes them with mid-latitude air in about 20-25 days. Due to the topography and land-sea thermal contrast, Rossby waves are more intense in the NH than in the SH than in the SH, where the polar vortex is very stable in the winter. This stability creates ideal conditions in the lower stratosphere for the destruction of ozone by CFC gases in the Antarctic spring, leading to the formation of the famous 'ozone hole'(Brasseur et al., 2005)[17].

Both the troposphere and the stratosphere may exhibit strong westerly winds that isolate polar air. In the troposphere, the polar region is colder than the mid-latitudes at all seasons, and thus the zonal thermal wind called 'the polar jet' also exists throughout the year, if somewhat weaker in the summer. The polar jet encircles the polar region between 40 and 60 degrees latitude, exhibiting significant meandering partly due to differential heating of land masses and oceans. In contrast, the stratospheric polar vortex exist only in the winter. During this season, the absence of sunlight inhibits ozone photolysis, the stratospheric heating mechanism, and creates a substantial temperature difference between the sunlit and the dark regions. In the summer, the temperature gradient is smaller, and the polar vortex breaks down. In the northern hemisphere, the polar vortex is sometimes prone to disturbances even during winter. Rossby waves that propagates from below may

weaken and sometimes reverse the westerly wind. The vortex may then be either displaced or split in two, allowing the cold polar air to escape and cause abnormally cold weather at lower latitudes. This phenomenon is called a 'Sudden Stratospheric Warming', and tends to occur about once every two or three years.

2.2 Stratospheric chemistry

The atmosphere consists of about 78 percent nitrogen, 21 percent oxygen, and 1 percent argon, in addition to numerous trace gases, of which the most important are shown in table 1. The abundance of a gas is most commonly expressed as a volume mixing ratio. For an ideal gas, this is simply a ratio between the number of gas molecules and the number of air molecules for a given volume. Useful units for trace gases are ppmv and ppbv(parts per million/billion by volume). Number density is the number of molecules over volume, usually expressed as $particles/cm^3$. The number density is useful in calculating the reaction rate of chemical equations, but vary greatly with pressure. In contrast, the vmr stays fairly constant throughout the atmosphere for a well-mixed constituent.

Table 1: Trace Gases in Dry Atmosphere (in parts per million), excluding the noble gases. They are taken from the NOAA(https://www.noaa.gov/jetstream/atmosphere), with the exception of CO_2 which is updated to the value as reported by the UN environment panel(https://data.unep.org/climate/) in December 2023.

Trace Gas	**Concentration (ppm)**
Carbon Dioxide (CO_2)	422
Methane (CH_4)	1.70
Hydrogen (H_2)	0.53
Nitrous Oxide (N_2O)	0.31
Carbon Monoxide (CO)	0.10
Ozone (O_3)	0.07
Nitrogen Dioxide (NO_2)	0.31

2.2.1 The Chapman cycle

Three forms of oxygen exist in the stratosphere: atomic oxygen, dioxygen, and ozone. These compounds engage in continuous creation and destruction through chemical processes. Sidney Chapman was the first to explain the presence of the ozone layer by suggesting a mechanism for ozone production. Under the influence of UV radiation, dioxygen may dissociate into two oxygen atoms, via

$$O_2 + hv(\lambda < 242.4nm) \longrightarrow 2\,O(j_2), \tag{4}$$

where hv is a photon of sufficient energy. The photo-dissociation rate j_2 will be further explained later in this section. Atomic oxygen is an essential ingredient to form ozone, and reacts rapidly with molecular oxygen as follows:

$$\mathrm{O} + \mathrm{O_2} + \mathrm{M} \longrightarrow \mathrm{O_3} + \mathrm{M}(k_2), \tag{5}$$

where M is an arbitrary air molecule. Next, two reactions are responsible for ozone destruction: photolysis via

$$\mathrm{O_3} + hv(\lambda < 1180nm) \longrightarrow \mathrm{O_2} + \mathrm{O}(j_3), \tag{6}$$

and the slow recombination with atomic oxygen,

$$\mathrm{O_3} + \mathrm{O} \longrightarrow 2\,\mathrm{O_2}(k_3). \tag{7}$$

The reactions of this Chapman cycle may be used to predict a vertical profile of ozone in the atmosphere. The production and loss terms of ozone and atomic oxygen may be expressed as

$$\frac{\partial[O_3]}{\partial t} = k_2[O][O_2][M] - j_3[O_3] - k_3[O][O_3] \text{ and} \tag{8}$$

$$\frac{\partial[O]}{\partial t} = 2j_2[O_2] + j_3[O_3] - k_2[O][O_2][M] - k_3[O][O_3], \tag{9}$$

where $[X]$ is the number density of X. When the stratosphere is illuminated, there is a rapid conversion between atomic oxygen and ozone, and the rate of change for odd oxygen(O_x),

$$\frac{\partial[O_x]}{\partial t} = \frac{\partial[O_3]}{\partial t} + \frac{\partial[O]}{\partial t} = 2j_2[O_2] - 2k_3[O][O_3] \tag{10}$$

is a convenient measure. By imposing the steady state condition on (9) and (10) and noticing that $j_3 >> k_3[O]$ in the stratosphere, a resulting expression for the density of ozone may be obtained as

$$[O_3] = [O_2]\left(\frac{j_2 k_2[M]}{j_3 k_3}\right)^{\frac{1}{2}}. \tag{11}$$

The photo-dissociation rates j_X has to be calculated carefully as they depend on the incident flux of solar photons, the frequency, and the properties of the molecule. For a frequency interval, the contribution to j_X is

$$dj_{Xv} = \Phi_{Xv}\sigma_{Xv}\left(\frac{F_v^{\downarrow}}{hv}\right), \tag{12}$$

where σ_{Xv} is the absorption cross section of molecule X. The quantum yield Φ_{Xv} is often accurately described by the step function. The spectral irradiance $F_v^{\downarrow}$ is the number of photons in the given frequency interval crossing unit horizontal area per unit time, and therefore depends on the path of the solar beam. The total photo-dissociation rate is found by integration over the frequencies v(Andrews, 2010). The path through the atmosphere depends on the solar zenith angle, defined as the angle between the vertical direction and the rays of the sun. For oxygen to be photo-dissociated, a photon of wavelength less than $242nm$ is required, while ozone is photo-dissociated up to $1180nm$. Consequently, j_2 requires a smaller solar zenith angle to be non-zero, while reaction (6) is active even at twilight.

The rate coefficient k_3 belongs to a bimolecular reaction, and as most such reactions, it is well approximated by the empirical Arrhenius expression,

$$k_3 = \alpha \exp(-\frac{E_a}{RT}) = 8.0 * 10^{-12} \exp(-2060/T), \tag{13}$$

where R is the universal gas constant, and E_a is the activation energy. For a termolecular reaction like (5), a third inert body M is required to carry away the excess energy of the reaction, and thereby conserve momentum. As this requires three molecules to collide, it is far less likely to occur than a bimolecular reaction with the same activation energy. The expression is given as a combination between the high pressure limit k_{inf}, and the low pressure limit k_0. For (5) however, it is sufficient to consider the low pressure limit, shown below.

$$k_2 = k_0^{298} \left(\frac{298}{T}\right)^n = 6 * 10^{-34} \left(\frac{298}{T}\right)^{2.4} \tag{14}$$

The vertical daytime ozone profile predicted by Chapman is too large compared to observations, as both transport and catalytic destruction cycles are neglected (Andrews, 2010). As the equator receives more sunlight than the polar regions, this is where the bulk of ozone production occurs. The Brewer-Dobson circulation therefore contributes as an ozone sink in the tropics, and as a source in the polar regions.

2.2.2 Catalytic cycles

The ozone concentration may be significantly reduced by the presence of ozone-depleting catalytic species. A catalyst is an effective way of removing odd oxygen as its own concentration is unaffected by the reaction. In the stratosphere, the main catalysts are odd-nitrogen (NO_x), odd-hydrogen (HO_x), Chlorine (Cl) and Bromine Br. Below follows an example of a catalytic cycle, with X as the catalyst.

$$\mathrm{X} + \mathrm{O_3} \longrightarrow \mathrm{XO} + \mathrm{O_2}\ (k_{x1}) \tag{15}$$
$$\mathrm{XO} + \mathrm{O} \longrightarrow \mathrm{X} + \mathrm{O_2}\ (k_{x2}) \tag{16}$$
$$\text{net: } \mathrm{O_3} + \mathrm{O} \longrightarrow 2\mathrm{O_2} \tag{17}$$

Adding this to the pure oxygen chemistry scheme modifies the vertical ozone profile of Chapman((11)). Assuming steady state, and that the catalytic reactions are slower than the fast conversion between O_3 and O in equations (5) and (6), the following modification of the ozone profile is obtained:

$$[O_3] = [O_2]\left(\frac{j_2 k_2 [M]}{j_3 k_3}\right)^{\frac{1}{2}} - [O_2]\frac{k_{x1} k_2 [X][M]}{2 k_3 j_3}. \tag{18}$$
$$= [O_2]\left(\frac{j_2 k_2 [M]}{j_3 k_3}\right)^{\frac{1}{2}} - \frac{k_{x2}[XO]}{2 k_3}. \tag{19}$$

Interestingly, the second term represents the competition between two loss mechanisms for odd oxygen. Adding more than one catalyst will complicate the picture. Their effect can not be added linearly, as the cycles may interact with each others; reservoir species such as HCl and $ClONO_2$ may temporarily tie up the catalysts, making them unavailable for reactions. The reservoir species are prone to photodissociation, and are therefore most abundant at nighttime, while the active species are present in daytime. Furthermore, the catalytic cycles run on atomic oxygen, which are scarcely found in the stratosphere at night, as essentially everything turns into ozone at twilight. Due to these factors, the catalytic species primarily contribute to ozone depletion in an illuminated atmosphere.

The impact a given ozone-depleting species may have on ozone depends heavily on its life-time. For the compound X, the lifetime is defined as

$$\tau_a = \frac{[X]}{|\frac{\partial [X]}{\partial t}|}. \tag{20}$$

In an oxygen-only atmosphere, the lifetime of ozone and atomic oxygen is a few minutes only, but the life-time of odd-oxygen is of the order of weeks. Similarly the lifetime of NO_x greatly exceeds that of N, NO and NO_2. The chemical lifetime generally decreases with height, as the solar photons have a longer path, and thus an increased chance of being absorbed before reaching low altitudes. The lower stratosphere is therefore a region under dynamic control. Figure 4 shows the photochemical lifetime of odd oxygen, as well as the regions of dynamic or chemical control.

The source of HO_x in the stratosphere is mainly CH_4 or H_2O from the troposphere, becoming oxidised or photolysed as it reaches the stratosphere. In the mesosphere

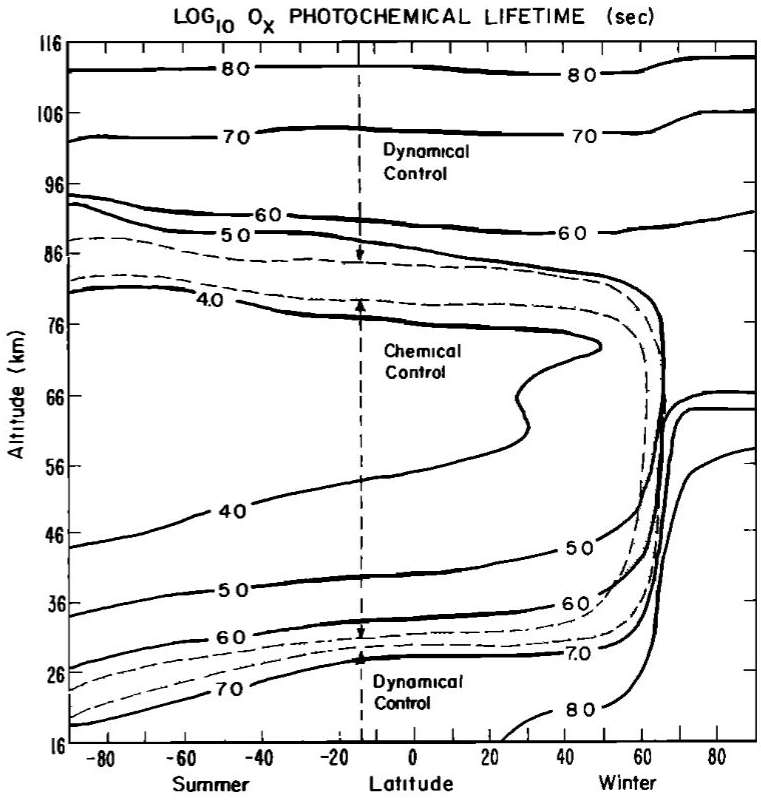

Figure 4: Shows the photo-chemical lifetime of odd oxygen, as well as the regions of dynamic or chemical control. From Garcia et Solomon (1985) [18].

and upwards, ionization of H_2 by galactic cosmic rays or solar proton events becomes the dominant source. As for catalytic ozone-deletion, the HO_x cycle makes an impact in the mesosphere, the lower stratosphere and in the troposphere(Brasseur et al., 2005).

The bulk of NO_x is created from oxidation of N_2O at low latitudes around 30 km and the concentration decreases moving polewards [17]. N_2O is present in the troposphere, and is injected into the stratosphere in the upward phase of the Brewer-Dobson circulation. Since pre-industrial times, the volume mixing ratio N_2O has increased from about 270ppbv to 315ppbv. However, the consequences for production of NO_2 is uncertain, as the global budget of neither N_2O nor NO_2 are well quantified(Brasseur et al, 2005). Ionization of N_2 by solar and galactic high energy particles is a minor source in the tropics, but becomes significant in the polar regions where the flux of particles are higher, and the abundance of NO_x is lower. In the presence of a solar proton event, production by ionization of N_2 increases significantly.

The sinks of NO_x are mainly reactions that form nitric acids:

$$NO_2 + OH \longrightarrow HNO_3 \tag{21}$$

$$N_2O_5(g) + H_2O(l, s) \longrightarrow 2HNO_3. \tag{22}$$

The second reaction occurs on the surface of particulates, for instance on sulfate aerosols or on polar stratospheric clouds(PSCs), which may form in temperatures lower than 190K(Brasseur et al.,2005). This type of reaction dominates in the winter, when the OH concentrations are low. Nitric acid is then transported down to the troposphere, where it undergoes removal by precipitation.

By far, the largest source of stratospheric halogens is a result of anthropogenic pollution, in particular chlorofluorcarbons(CFCs). These gases were patented in 1928 and became widely used as refrigerants and propellants. Designed to be chemically inactive, their catastrophic effect came as a surprise. As they eventually mixed into the stratosphere, the short-wave radiation allowed for photo-dissosiaction, creating the reactive catalytic species ClO and Cl. Fortunately for the ozone layer, the bulk is tied up in reservoir species, in particular $ClONO_2$, and the global ozone depletion due to gas-phase reactions is modest. In 1985, a paper was published by Farman et al.[19], revealing a dramatic spring time ozone depletion over the Halley Bay in Antarctica. They pointed out how the reaction

$$HCl + ClONO_2 \longrightarrow Cl_2 + HNO_3 \tag{23}$$

was very effective in the cold antarctic stratosphere, where PSCs are present. This reaction does mainly two things. Firstly, chlorine is liberated, and secondly, NO_x is removed. Consequently, the fraction of active chlorine increases, causing an effective ozone-depletion. As mentioned, the catalytic cycles shown in (17) depend on atomic oxygen. The low solar zenith angle of the polar spring does not produce sufficient atomic oxygen to cause the observed ozone loss. Rather, the following chlorine peroxide cycle was showed to be responsible for more than two thirds of the ozone loss, with bromine cycles accounting for most of the remaining loss(Molina et al., 1996)[20].

$$ClO + ClO + M \longrightarrow Cl_2O_2 + M \tag{24}$$
$$Cl_2O_2 + h\nu \longrightarrow 2Cl + O_2 \tag{25}$$
$$Cl + O_3 \longrightarrow ClO + O_2 \tag{26}$$

Bromine is very similar to chlorine and tend to make the same chemical connections, but less tightly bound. As the reservoir species for bromine is easier to break, a greater factor of active bromine can be found, making it about 50 times as effective as chlorine. However, it is outnumbered by chlorine by a factor of 300, so the altogether effect on ozone is lower.

An ozone column below 220 DU had never been recorded prior to the year 1979, but the 90s hosted several years with a minimum below 100 DU, as reported by NASA Ozone Watch[21]. In 1987, the first international agreement to phase-out the use of CFCs was put into action, and with the subsequent amendments, emissions declined rapidly. Due to a lifetime of about 100 years, the effects of the pollution remained. The amount of CFC gases reached its maxima in year 2000, and has

been decreasing steadily the last 20 years; the accumulated pollution is now 30 percent less than at its peak(with the 1980 amount as the zero reference). At the same time, the antarctic ozone hole shows a weak trend towards recovery, in spite of low measurements the recent years. Surprisingly low values of year 2020 and 2021 may be attributed to the forest fires in Australia in august 2020, and the eruption of La Soufrière in 2021. Both these events would lead to an increased amount of particulates over the antarctic, increasing the fraction of reactive chorine (Yook et al. 2022)[22]. The eruption of Hunga Tonga-Hunga Ha'apai in January 2022 was the greatest since that of mount Pinatabu in 1991, which caused a record low ozone column in 1992.

A model study by Egorova et al.(2023)[23] suggest that without the Montreal Protocol, and with uncontrollable increases in ozone-depleting halogens, the ozone layer would be almost entirely depleted in this century, along with a massive speed-up of the global warming, causing the arctic to be ice free about 40 years earlier. This highlights the importance of this protocol, serving as a golden example of an event where all countries urgently agreed upon measures to protect the planet.

2.2.3 Distribution of ozone

Stratospheric ozone is controlled by both photo-chemistry and transport, the former being most prominent in the tropics, and the latter dominating in the polar winter regions. Here, the seasonal pattern is ozone buildup due to transport during winter, and a decline during summer and autumn due to photo-dissociating of ozone. Consequently, the greatest annual variations in total ozone column are found in the polar regions, as transport may vary from year to year, while the incoming flux of solar photons stays fairly constant. Year-to-year variability peaks in March, and it has been recorded arctic monthly mean values as high as 525 DU and as low as 325 DU. August is the month with lowest annual variability globally, with year-to-year changes of less than 25 DU(Fioletov et al., 2008)[24].

The total vertical ozone column has clear annual variations at higher latitudes. A surface plot of the zonally averaged total ozone as a function of month of year and latitude is shown in figure 5. Showing the average from 1964-1980, the following descriptions will reflect the ozone distribution of an atmosphere unperturbed by the CFC gases, and thus without the springtime ozone hole. The polar regions exhibit the largest month-to-month variations, dominated by the abundance of springtime ozone in the NH. This ozone maxima has some longitudinal dependence, being located over the Canadian arctic and eastern Siberia. The dark of winter inhibits ozone destruction by (6), and allows transported ozone to accumulate. As the Brewer-Dobson circulation is stronger in the NH due to larger planetary-wave amplitudes, the SH spring maxima has a lower amplitude. In the autumn, the two hemispheres display similar amounts, suggesting a larger degree of photochemical control(Fioletov et al., 2008).

The short-term ozone fluctuations are also greater at higher latitudes, where the standard deviations of the daily values from the annual cycle are 12-15 percent in winter-spring and 7-8 percent in summer-autumn. In the tropics, the daily depar-

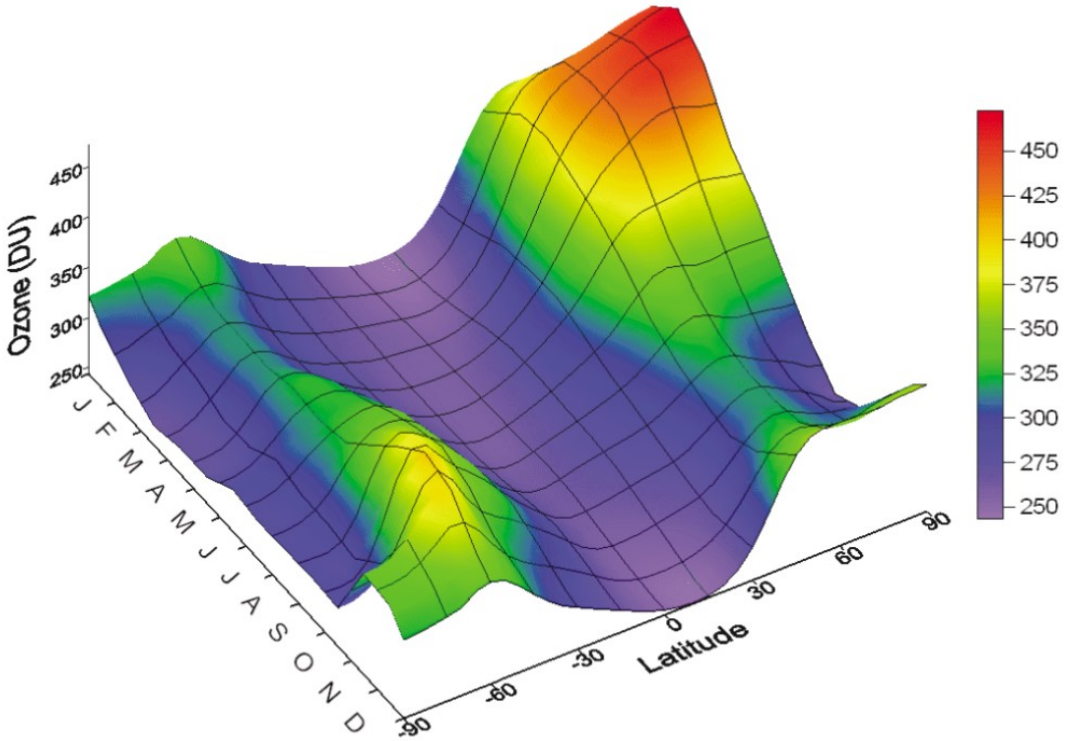

Figure 5: Surface plot of zonal monthly mean total ozone as a function of latitude and month estimated from ground based data for the period 1964-80. From Fioletov et al.(2008).

ture from the annual cycle is about 3-5 percent(Fioletov 2018). The diurnal variations of stratospheric ozone are small, and mostly restricted to the upper tropical stratosphere. Sakazaki et al.(2013)[25] found the peak-to-peak difference in ozone mixing ratio to be about 8 percent in this region, while the total column ozone stayed within 1 percent. At sunset, essentially all atomic oxygen recombines into ozone, but where $O_x \simeq O_3$, this contribution is negligible. The diurnal cycle can be attributed to both dynamics and chemistry, in particular the vertical tidal waves and the diurnal cycles of HO_x and NO_x(Sakazaki et al., 2013).

2.3 Solar Proton Events

As seen in the introduction, solar proton events may cause serious perturbations to the chemistry of the atmosphere. The possibility of earth being struck by violent solar storms pose several additional questions: How do they form, and is it possible to predict them? How often do they occur, and is there an upper bound of greatness? What are the consequences for the society? To better understand the mechanisms causing such events, there will be a quick detour into the fascinating magnetic behaviour of the sun, before presenting the solar wind, coronal mass ejections and solar flares, and how they interact with Earths atmosphere.

2.3.1 The sun's magnetic behaviour

The sun contains about 99.8 percent of the mass in the solar system, but is losing weight at a rate of about 4 million tons per second, by converting mass into energy. Nuclear fusion in the core of the sun releases radiation that works its way up to the surface and propels convective motions just below the photosphere, the surface layer. This layer is the lowest and densest part of the solar atmosphere, maintaining a temperature of about 5800 Kelvin. It may be approximated as a black body and radiates with a peak in the visible spectrum. Above the photosphere lies the chromosphere, a highly irregular and stormy layer containing spikes and prominences. The corona extending above may reach temperatures of a few million Kelvins and radiates with a peak in the X-rays. At such temperatures, the particles' energies may overcome the sun's escape velocity, and thus a diffuse solar gas covers the seemingly empty space of the solar system.

The sun's magnetic fields consist of smaller scale intense fields associated with the sunspots(strength of max 3kG), and a weaker global field(strength of max 6-12 G), called the interplanetary magnetic field(IMF). Much is yet to be understood about the mechanisms creating these, but it is generally agreed upon that the electrical currents in the Sun's convection zone act as a dynamo.

The solar wind is a constant stream of electrons and ions escaping the sun. In 1958, Eugene Parker showed that the solar wind carried both the sun's particles and the magnetic fields to the far reaches of the solar system. He also concluded that the magnetism had the shape of an Archimedean spiral, with one end rooted in the sun, confirmed by observations in 1963(Lang et al.,2008)[26]. This spiral shape is caused by the sun's rotation and coils the magnetism, causing it to fall by a factor of $R^{-1.4}$ instead of the quadratic relation one could expect. The density of the solar wind behaves similarly, but fills a greater volume, and thus falls off by a factor of $R^{-1.86}$. The solar wind may be categorized into two types, with two different sources. The fast solar wind originates from the polar region of the sun, and from coronal holes, while the slower has its origin in the corona. The properties of the IMF vary with the solar cycle, and the field is strongest at solar maximum.

The variation in the emergence of sunspots was discovered by Samuel Heinrich Schwabe in the early 1840s. At solar maxima, about 100 spots may be seen simultaneously, while at solar minima, there might be periods for as long as a month with no spots at all (Lang et al.,2008)[26]. The number of sunspots follows a cycle of 11.1 years on average. Sunspots break out in middle latitudes, in a belt parallel to the equator between 45 to 30 degrees, and move down towards lower latitudes as the cycle progresses. They tend to travel in pairs of opposite polarity, joined by magnetic loops that rise above the photosphere into the corona, known as coronal loops. The magnetized atmosphere is then called a solar active region. Eventually, the sunspots approach the equator and disappear, before reappearing in the middle latitudes at the start of the next cycle. The polarity of the IMF changes for each new cycle, indicating that the sun's full magnetic cycle is 22.2 years on average.

Moving into the field of magnetohydrodynamics(MHD) a fascinating behaviour in

the sun's atmosphere may be shown. For length scales relevant to magnetic structures in the sun, the conductivity may be approximated as infinite(Mullan et al., page 267, 2010)[27], and we reach what is called the limit of magnetohydrodynamics. In this limit, what remains of Maxwell's equations are

$$\frac{\partial \vec{B}}{\partial t} = \nabla x(\vec{V} x \vec{B}), \tag{27}$$

where B is the magnetic field, and V is the velocity field of the plasma. From this, it may be shown that for a parcel of plasma in a magnetic field, the magnetic flux neither enters nor leaves the parcel as it moves. Thus the field and the gas are forced to move together, commonly described as 'frozen together'. As a consequence, in the presence of a strong magnetic field, the gas must follow the field lines, and perhaps more surprisingly; if the gas pressure is greater than the magnetic pressure, the field must follow the motions of the gas. Thus, when the plasma of the photosphere is subject to convective motions, the magnetic field lines experience twisting and stretching, and a reservoir of magnetic energy builds up as the stress and tension increase(Mullan et al., 2010). This stored energy can be suddenly released in a process called magnetic reconnection.

Magnetic reconnection is initiated when two plasma regions with opposing magnetic fields approach each other. This creates a region where a plasma sheet builds up, and the total magnetic field is close to zero. When the particles move close to this region, the gyroradius increase as the field weakens. When the gyroradius is larger than the distance between the two opposing fields, the assumption of MHD breaks down, and previously trapped particles may escape. The field lines with opposing fields approach each others, and as they lean in for the kiss, the original lines break in two, and reconnect with the lines of the opposing field. This forms a magnetic field perpendicular to the original motion of the plasma. The resulting field is weaker, as the magnetic energy has been transformed into kinetic and thermal energy, which accelerates electrons and heats the corona.

2.3.2 Earths magnetic field

Earth's magnetic field at high altitudes is a dipole, with the south magnetic pole close to the geographic north pole, and the north magnetic pole close to the geographic south pole. The main source of this intrinsic field is the convective currents in the metallic liquid core of the Earth, but ionospheric and magnetospheric currents also contribute to the formation of the magnetosphere, the Earth's magnetic shield. The magnetopause is the boundary between the magnetosphere and the surrounding plasma, located at the point of hydrostatic equilibrium between the pressure of the magnetic field and the solar wind. Depending on the strength of the solar wind, the magnetopause is found in a distance ranging from 10 RE to about 3 RE under extreme conditions.

The magnetosphere is shaped by the solar wind, which pushes it into a bullet-like shape, with a flat field on the dayside, and a long tail on the night side, see figure

6. Between the lines that stretch towards the day and night side, there is a region where the lines are connected to the IMF, called the cusp region. This formation of open field lines enables particles to travel directly from the sun to the polar regions. As the IMF forms an Archimedean spiral, the polar region of the Earth is connected to the western hemisphere of the sun and is thus more sensitive to solar activity occurring in this region. However, the most common way for solar particles to enter our atmosphere is through magnetic reconnection. This process may occur when Earth's magnetic field and the field carried by the incoming charged particles are directed opposite of each other. After the lines have reconnected, this forms an open system where particles and energy are free to move from the IMF and into Earth's atmosphere.

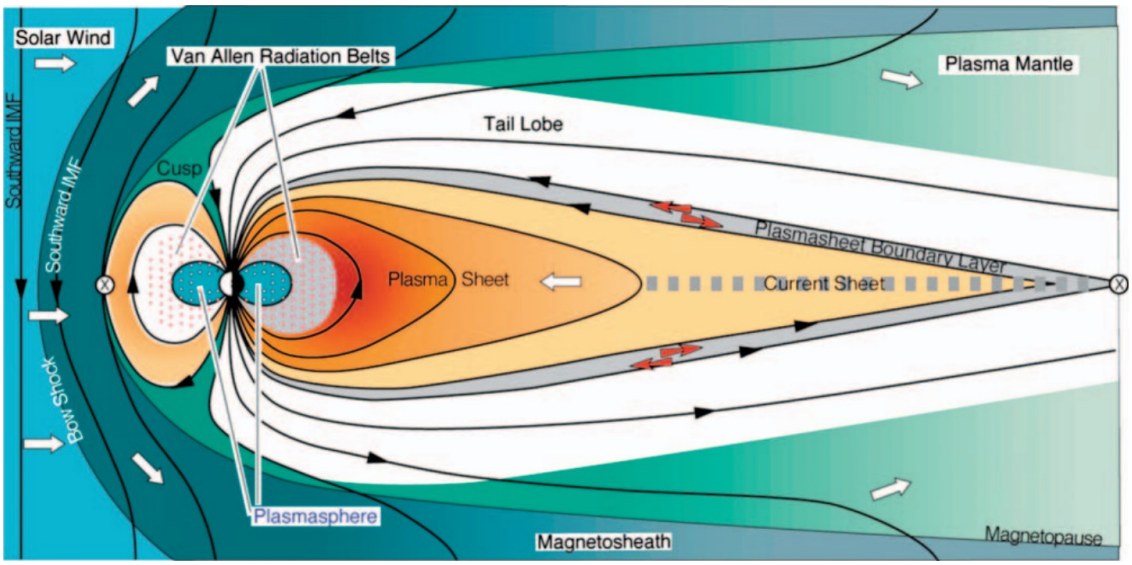

Figure 6: Cross section of the simplest model of the magnetosphere. If the interplanetary magnetic field(IMF) has a southward orientation, it interacts with earths northward magnetic field in a process of magnetic reconnection, allowing solar particles to enter the terrestrial atmosphere. From http://space.rice.edu

2.3.3 Coronal mass ejections

Solar active regions are areas of enhanced magnetic activity, which generates a plethora of emissions, including solar X-rays, solar radio emissions, solar plasma, energetic solar particles, and coronal mass ejections(Shea, 2012)[28].

Coronal mass ejections(CMEs) are sudden outflows of massive magnetic blobs containing solar particles. The topology of the magnetic blob is uncertain, as it may vary from event to event, and may resemble bubbles, ropes or loops, and be with or without an attachment to the suns photosphere. Their origin are often magnetic flux tubes in the solar corona that erupt and reconnect, and launch massive amounts of energetic particles in the direction perpendicular to the magnetic field. However, the exact mechanisms for accelerating the particles, and even what layer of the solar atmosphere this occurs, remains uncertain(Akasofu,2011)[29]. The blob of particles is observed to contain velocities ranging from about 300 - 2000 km/s,

and it quickly expands to become larger than the sun itself(Lang et al.,2008)[26]. If the velocity is larger than that of the solar wind, the CME ploughs particles in front of it like a piston, increasing the particle pressure. Furthermore, if the speed difference exceeds the magnetic sound speed, a shock wave is formed. These fast CMEs reach Earth in about 1-2 days, while the ones moving slower than the solar wind take about 3-4 days to arrive. One of the proposed mechanisms for further accelerating the particles is by means of solar flares, a phenomenon often associated with CMEs. Similar to CMEs, they are caused by the sudden release of magnetic energy from the solar active regions. The flares consist of intense bursts of radiation, primarily in the X-ray and visible spectrum, and last from minutes to hours. Although both solar flares and CMEs may occur independently, large CMEs tend to be accompanied by solar flares and vice versa(Lang et al., 2008).

The CME will have a different effect on the atmosphere depending on the location of the outburst. Solar proton events occurring as a result of solar activity located between 90°East and 30°West may be classified as 'interplanetary shock dominated events', and the ones occurring in the western hemisphere are called 'near-sun injection events'(see figure 7). The former is caused by a CME travelling in a direct line from the sun to the Earth. If the velocity is greater than that of the solar wind, this will produce shocks which further accelerate the ions. As Earth's magnetic field is directed northwards, the incoming blob of particles must carry a field of southward orientation in order to cause a geomagnetic storm. This orientation allows for magnetic reconnection, and thus a greater transfer of energy and particles into the magnetosphere. The "near-Sun injection events" occur when there is a direct magnetic connection between the Earth and the ejection site on the sun. Due to the spiralling interplanetary magnetic field, this only occurs for longitudes further West than 30 degrees. This connection provides a highway for the accelerated particles, as charged particles experience little resistance when travelling along magnetic field lines. Solar proton events with a hard energy spectrum are often associated with this type of event, with a rapid increase in the proton flux followed by a slow decrease over the next one or two days. The 'interplanetary shock dominated events' display a softer spectrum with a slow buildup, that intensifies as the shock reaches Earth(Shea et al., 2012).

Solar proton events may be referred to as Ground Level Events(GLEs[1]) if the particles hold enough energy to produce measurable effects at Earths surface. Such events must have a harder energy spectrum, and is often associated with activity on the westerly portion of the solar disk. In fact, 53(76%) of the 70 GLEs identified between 1942 and 2006, had its 'parent activity' further west than 30°(Shea et al.,2012).

2.3.4 Effects of solar proton events

The NOAA Space Weather Prediction Center defines a solar proton event as having a flux of $> 10\,\mathrm{MeV}$ protons greater than $10\,\mathrm{particles\,(cm^2\,s\,sr)^{-1}}$. To penetrate into the stratosphere, the range of energies must exceed $100\,\mathrm{MeV}$. If the ionization is

[1]Sometimes referred to as Ground Level Enhancement(GLE).

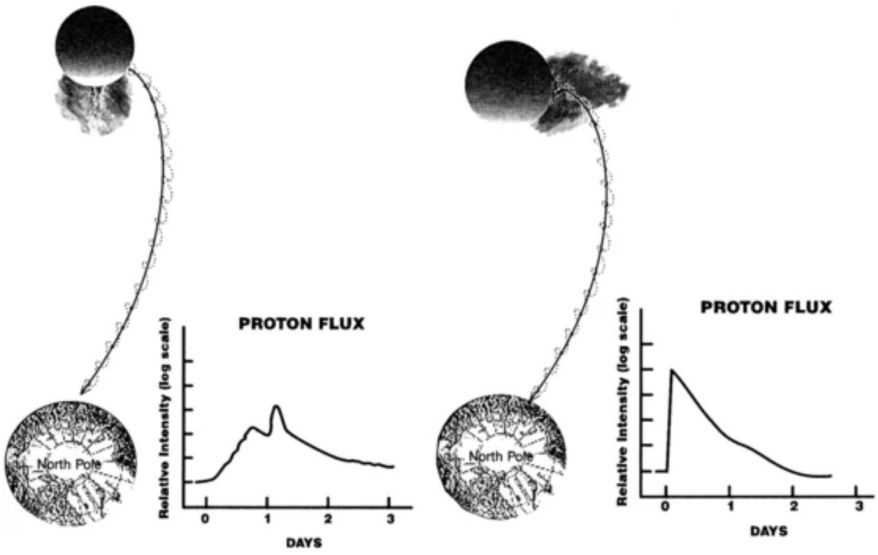

Figure 7: Conceptual view of two types of solar proton increases typically observed at Earth. The left side portraits events associated with solar activity near the central meridian of the sun, where the "additional proton flux increase" displays the effect of an interplanetary shock as it passes by Earth. The right side shows activity on the western side of the sun, where a direct magnetic connection to earth is possible. From Shea et al.(2012) [28].

sufficiently hard to be detected at the Earth's surface (450 MeV), the event may be referred to as a Ground-level event (GLE)(Shea et al.,2012). Solar Proton Events are hard to predict, but changes in soft X-rays and proton fluxes in the hours before an event have been used to develop statistical prediction models. State-of-the-art models can provide a probability of detection of about 0.80 (with a false alarm probability of 0.26), with an average warning time of 2.6 hours in advance (Zhong et al., 2019) [30].

The solar particles deposit their energy in the polar cap, as this is the region with the weakest geomagnetic shielding. It is common to assume a uniform longitudinal distribution, but for particles in the 1-20 MeV range, a strong day-night asymmetry is present. Due to perturbations in the magnetospheric currents systems during a geomagnetic storm, the latitudes receiving the bulk of the energetic particles are pushed towards the poles in the daytime, and towards the equator in the night-time(Tyssøy et al., 2014) [31]. Figure 8 shows which altitudes receives the bulk of the energy from a solar protons events.

As the energetic particles penetrate into the atmosphere, they will eventually collide and deposit their energy, resulting in the ionization of nitrogen and oxygen through the following procedure, following Calisto et al.(2012 [4]). Firstly, the energetic protons ionize nitrogen and oxygen as

$$\mathrm{O}_2 + p \longrightarrow O_2^+ + p + e* \tag{28}$$
$$\mathrm{N}_2 + p \longrightarrow N_2^+ + p + e*, \tag{29}$$

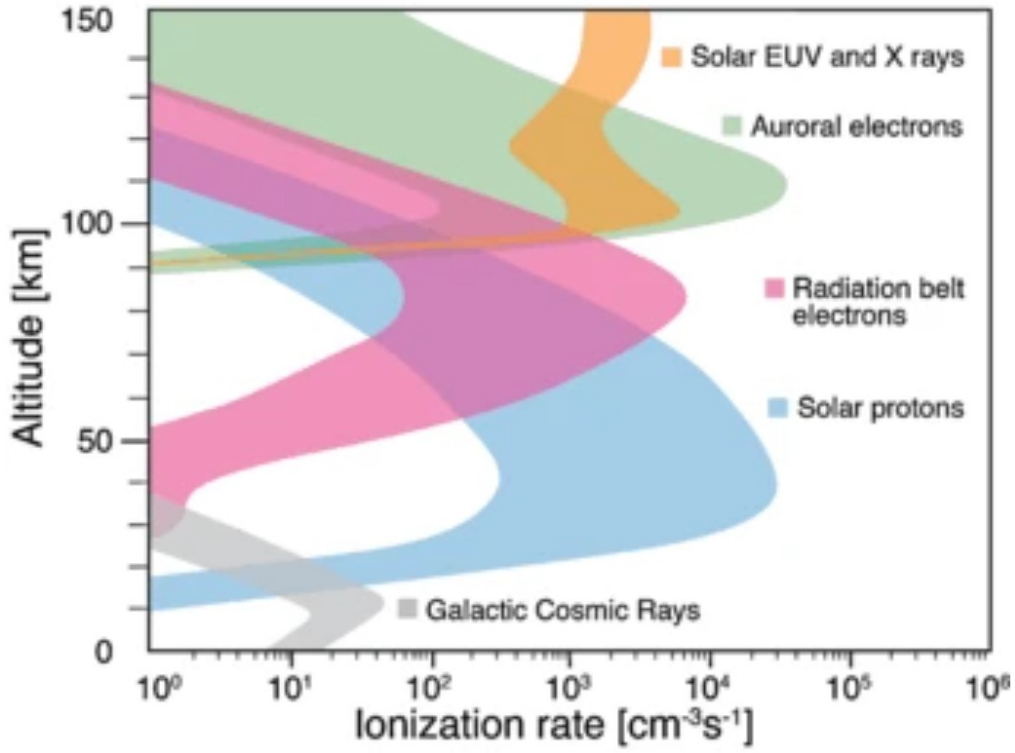

Figure 8: Instantaneous ionization rates of EPP, Solar EUV and X rays in Earth's atmosphere. Originally from Baker et al.(2012) [32], modified by Mironova et al.(2015) [33].

where $e*$ is secondary electrons with high kinetic energy. These electrons may deposit their energy by exiting nitrogen as

$$\mathrm{N}_2 + e* \longrightarrow 2N(4S; 2D) + e, \tag{30}$$

where 4S is the ground state, and 2D is the electronic first exited state. Almost all the exited nitrogen reacts with oxygen to produce NO_x via

$$N(2D) + \mathrm{O}_2 \longrightarrow \mathrm{NO} + O. \tag{31}$$

The ground state, however, leads to almost immediate destruction of NO_x through the reaction.

$$N(4S) + NO \longrightarrow \mathrm{N}_2 + \mathrm{O}. \tag{32}$$

This highlights the effect the partitioning between N(4S) and N(2D) will have on the total production. In 1976, Porter et al. [34] provided a reasonable guess for the amount of atomic nitrogen produced per ion pair, as well as a branching ratio. One ion pair is assumed to produce about 0.69 N(2D) and 0.56 N(4S).

Below the mesopause, in the presence of water cluster ions, the solar protons will also initiate the formation of odd hydrogen. In the upper stratosphere and lower

mesosphere, one ion pair is calculated to produce approximately 2 HO_x species, and a little less in the upper mesosphere(Solomon et al.,1981[35]). Both HO_x and NO_x destroy ozone through catalytic cycles, and consequently, the radiative balance of the middle atmosphere is disturbed after such events.

We have seen here and in the introduction that solar proton events may cause changes to the chemistry in the middle atmosphere. However, it is important to note that during a solar proton event, the most significant disruptions occur in the ionosphere. The accompanying X-rays lead to additional ionization in the sunlit portion of the atmosphere, while energetic particles induce extra ionization in the polar cap. This heightened ionization can result in partial or total absorption of high-frequency signals, posing a challenge for communication, particularly for aircraft reliant on this communication method(Shea et al., 2012).

Spacecraft operations may also by compromised by a higher flux of solar particles. Depending on the energy, it may either penetrate the devise, rending it irreparable, or deposit enough energy to change the electronic state of the device from 'off' to 'on'. The latter is called a soft error. Recently, it has been attempted to count these soft errors in spacecraft devices as a method of measuring solar particle activity in the solar system(Sanchez-Cano et al.,2023)[36]. The direct radiation encountered by commercial aircrafts is essentially harmless. During the Halloween storms in 2003, a dosimeter onboard a flight(Munich-Chicago) showed a dose increase of only 35%(Shea et al.,2012). The most dramatic direct effect for society is power loss caused by induced geomagnetic currents. During the solar proton event of September 1989, darkness filled the entire region of Quebec!

3 The use of atmospheric models

A plethora of models are used in atmospheric physics, ranging from the advanced 3D climate models, to simple chemistry models. The need for complexity in order to reproduce reality must balance the need to understand the driving mechanism behind the results. Additionally, the work of implementation and the processing time must also be taken into account. We distinguish between two methods of solving the physical equations; an Eulerian or a Lagrangian view. The Eulerian method employs a fixed coordinate system and treats the particle phase as a continuum, meanwhile in the Lagrangian method, the coordinate system follows a parcel of air as it moves. Eulerian models often maintain conservative properties, and are well-suited where the conservation of mass, energy, or momentum is crucial.

Three different models are employed to answer our question of how progressively larger solar storms affect the ozone layer. Presented first is a very simple nighttime chemistry box model. As this model proved to be insufficient to explain the observed ozone loss, MISU-1D is introduced, a more comprehensive chemical box model that includes photolysis as well. This model will be employed to find the ozone depletion as a function of increases in NO_y. Lastly, the most comprehensive climate model in use today, WACCM, is presented. Kalakoski et al.(2023)[9] recently made simulations of a hypothetical solar storm in 2012, scaled by 1,10 and 100 , and these datasets will be used to verify the results found with the simpler MISU-1D model. This section also describes how the models will be used, and which datasets are used.

3.1 A simple nighttime box-model

As a first step, we begin by creating a simple nighttime box model, with oxygen and nitrogen species as the only reactants. All dynamics and photolysis are neglected. To asses the model, the results will be compared with WACCM simulations of the Halloween event in 2003.

3.1.1 The differential equations

A nighttime box-model of the atmosphere consisting of only oxygen and nitrogen is governed by the chemical equations shown in table 2. These equations can be translated into a system of ordinary differential equations(ODEs),

$$\frac{d\mathrm{O}}{dt} = -\mathrm{O}\left(k_2\mathrm{O_2M} - k_3\mathrm{O_3} - b_3\mathrm{NO_2}\right) \tag{33}$$
$$\frac{d\mathrm{O_3}}{dt} = k_2\mathrm{O_2OM} - \mathrm{O_3}\left(k_3\mathrm{O} - b_4\mathrm{NO} - b_9\mathrm{NO_2}\right) \tag{34}$$
$$\frac{dNO}{dt} = b_3\mathrm{NO_2O} - b_4\mathrm{NOO_3} \tag{35}$$
$$\frac{d\mathrm{NO_2}}{dt} = b_4\mathrm{NOO_3} - \mathrm{NO_2}\left(b_3\mathrm{O} - b_9\mathrm{O_3} - b_{12}\mathrm{NO_3}\right) \tag{36}$$
$$\frac{d\mathrm{NO_3}}{dt} = b_9\mathrm{NO_2O_3} - b_{12}\mathrm{NO_3NO_2} \tag{37}$$
$$\frac{d\mathrm{N_2O_5}}{dt} = b_{12}\mathrm{NO_3NO_2}, \tag{38}$$

where the temperature-dependent reaction coefficients are given in table 2.

Now, we must make a distinction between two types of steady state: momentary steady state, and global steady state. The momentary steady state of ozone is reached when the concentration of ozone is equal to all sources divided by all sinks. As the source of ozone, namely atomic oxygen, drops to zero at night, the momentary steady state of ozone is 0, a state that is not reached. The global steady state is the vector of values the system converges towards as time evolves. This system of ODEs has a global steady state when $\mathrm{O} = \mathrm{NO} = \text{`}\mathrm{NO_2} = \mathrm{NO_3} = 0$. Ozone is thus free to take any value, and the equilibrium may be classified as an unstable manifold. That is, for a system in global steady state, any deviation from it will move $\mathrm{O_3}$ to a new equilibrium value. A time-dependent calculation is thus required to find the final state of $\mathrm{O_3}$ for some initial conditions. If the system is considered isolated, the final values must additionally obey the conservation of oxygen and nitrogen.

Chemical Equations			Rate Coeff.	Temp. Dependence
$\mathrm{O + O_2 + M}$	$\longrightarrow$	$\mathrm{O_3 + M}$	k_2	$(298/T)^{-2.4}$
$\mathrm{O + O_3}$	$\longrightarrow$	$\mathrm{2\,O_2}$	k_3	$\exp\left(-2060/T\right)$
$\mathrm{NO_2 + O}$	$\longrightarrow$	$\mathrm{NO + O_2}$	b_3	$\exp\left(-1500/T\right)$
$\mathrm{NO + O_3}$	$\longrightarrow$	$\mathrm{NO_2 + O_2}$	b_4	$\exp\left(120/T\right)$
$\mathrm{NO_2 + O_3}$	$\longrightarrow$	$\mathrm{NO_3 + O_2}$	b_9	$\exp\left(-2450/T\right)$
$\mathrm{NO_2 + NO_3 + M}$	$\longrightarrow$	$\mathrm{N_2O_5}$,	b_{12}	*

Table 2: Shows the chemical reactions that will be used in the nighttime chemistry box model with only oxygen and nitrogen. The symbol M means that a third body is required for momentum conservation. The rate coefficient for each reaction is also given, along with its temperature dependence. For b_{12} the temperature dependence depends on pressure.

3.1.2 Numerical simulation

The system of differential equations given by 38, is a so-called *stiff* system, as the life-time of different terms vary with several orders of magnitude. Table 3 shows the life-times calculated with average atmospheric conditions at 20 and $40km$. These life-times depend both on temperature, and on the concentrations of the species in the model. As the reactions with O occur on the scale of seconds, but the build-up of N_2O_5 takes weeks, the numerical method is adjusted thereafter. The system is solved using the Euler method with three different time-steps: $dt = 0.001$ in the first 30 seconds, $dt = 0.05$ in the next three hours, and $dt = 5$ in the next 40 days. These choices corresponds to the saturation of O, NO and NO_2, respectively. The initial conditions are the output from the SD-WACCM-D on 2nd November 2003, when the atmosphere is perturbed after the Halloween storms. The resulting plot 9 shows that, as mentioned, the dynamics of the system has three different phases corresponding to the saturation of the three species.

Species	Number Density, ρ_N		Lifetimes, τ	
	$20km$	$40km$	$20km$	$40km$
O	0	0	$10^{-2}s$	$1s$
O_3	$5 \cdot 10^{12}$	$4 \cdot 10^{11}$	$10^{10}s$	$10^{8}s$
NO	0	0	$100s$	$400s$
NO_2	10^{8}	10^{9}	$10^{6}s$	$10^{5}s$
NO_3	10^{5}	10^{7}	$10^{3}s$	$10^{4}s$

Table 3: Shows the approximate concentrations of O_x and NO_y at $20km$ and $40km$[17]. These values are used to calculate a crude estimate of the lifetime based on the system of equations in 38. NO and O is approximately 0 for this purpose. The temperature is estimated to be $208K$ at $20km$ and $240K$ at $40km$.

In the first phase, O may either turn into O_3, or into NO, which destroys O_3. What becomes of O is a function of temperature, pressure and amount of NO_2. In the second phase, NO reacts with O_3 to form NO_2. The third phase shows the slow reaction between NO_2 and O_3, along with the build-up of the nitrogen reservoir species.

The different scale of the life-times makes it possible to estimate what the steady state value of O_3 will be for some initial conditions. The amount of destruction of O_3 depends almost entirely on the third phase, when O_3 reacts with NO_2. The effect of the first two phases is therefore neglected. Moreover, NO_2 reacts faster with NO_3 than with O_3, motivating the assumption that all NO_3 reacts immediately with NO_2 to form N_2O_5. The final approximate value of ozone can thus be expressed as

$$O_{3,ss} = O_{3,0} - \frac{1}{2} NO_{2,0}, \tag{39}$$

where 0 denotes the initial values. The numerical simulations seems to approach this value in about 40 days.

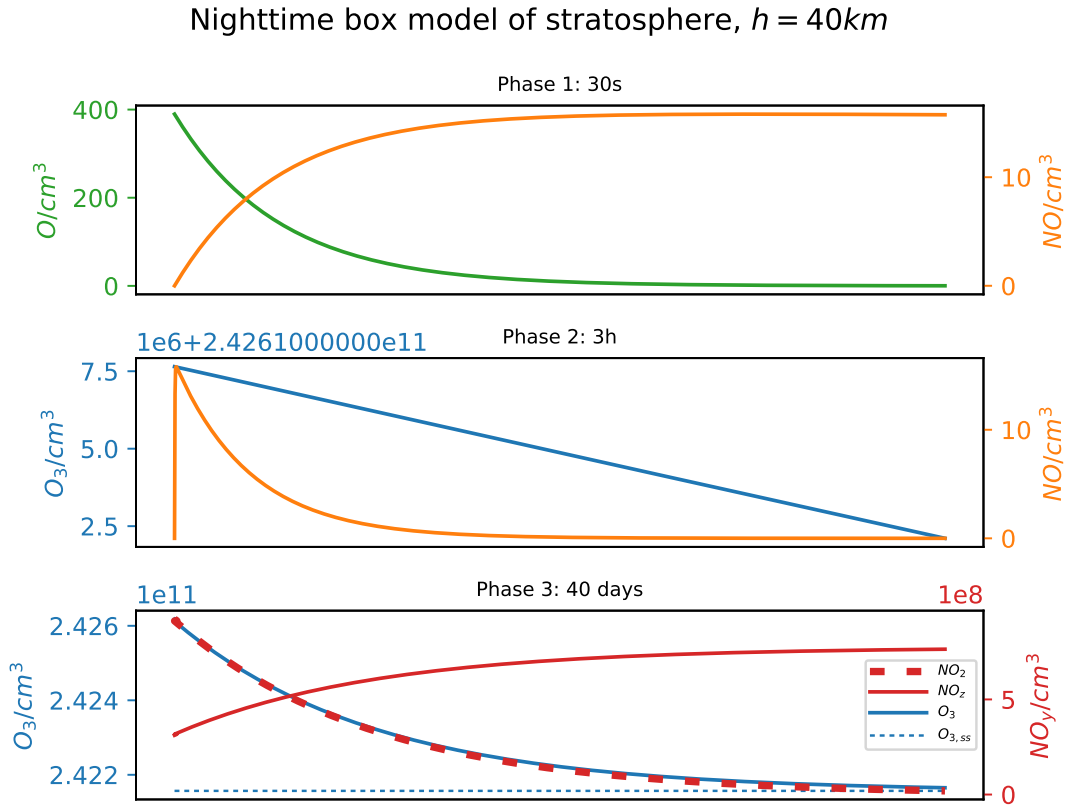

Figure 9: A box-model of the nighttime-chemistry at $40km$. The initial conditions are the output from the SD-WACCM-D on 2nd November 2003, when the atmosphere is perturbed after the Halloween storms. The model runs for 40 days without any new input.The three chemical species O(green), NO(orange) and NO_2(red dots) saturates with different time constants, leading to three different phases in the simulation. The lower panel show the build-up of reservoir species along with the depletion of ozone. NO_z is defined as NO_y-NO_x, and is equal to the sum of N_2O_5 and NO_3.

3.1.3 Comparing with SD-WACCM-D

The simple nighttime model is compared to the same event simulated by SD-WACCM-D, in order to assess how much the nighttime chemistry alone contributes to the ozone depletion. The data is sampled to fit with the measure points of MIPAS, and consists of a nightly value, averaged over all longitudes, and all latitudes between 60 and 90 degrees. For a more detailed version description, see Jia et al.(2020)[37]. In the simple nighttime model, the concentrations of NO_2, O and N_2O_5 are nudged each day to follow the SD-WACCM-D values of NO_x, O and NO_z($NO_z = NO_y - NO_x$). NO and NO_3 are set to 0 each day, as they are both short lived species, and will be created in reaction with O_x and NO_2. This method aims to reproduce the conditions of downwelling of NO_x and NO_y in the aftermath of the storm. All gaps in the SD-WACCM-D data are filled by its previous day. The comparison between the two models is presented in figure 10.

The ozone depletion of SD-WACCM-D is not well reproduced by the simple nighttime model, as it only accounts for a fraction of the ozone loss in the weeks following

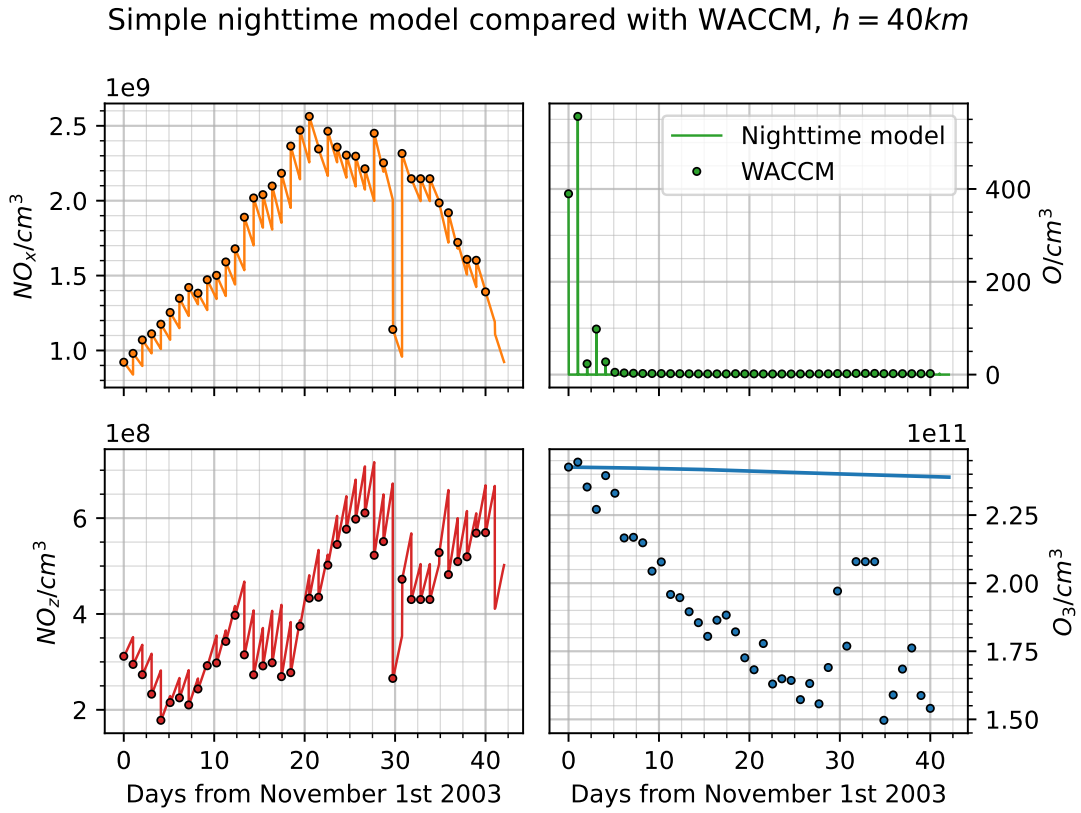

Figure 10: A comparison between SD-WACCM-D and a simple box-model of nighttime chemistry in the stratosphere after the Halloween event in 2003. The SD-WACCM-D data is a nightly average over all longitudes, and all latitudes between 60N and 90N. The values of NO_2, O and N_2O_5 in the simple nighttime model are nudged to follow the values of SD-WACCM-D, hence the zigzag-patterns.

the solar storm. One objection to this method is that the amount of atomic oxygen saturates in a few seconds, and consequently, the final results depend on the frequency of the 'nudging'. Physically, the nudging represent the chemical source due to downwelling. Should the level of atomic oxygen be forced to stay constant at 500 atoms per cubic centimeter for 24 hours, catalytic nitrogen destruction would be allowed to occur, and perhaps we would see a larger drop in ozone concentrations in the first days of simulation, when atomic oxygen is present. Nevertheless, the bulk of the ozone loss simulated by SD-WACCM-D takes place about 20 days later, when NO_x has reached its max value. This distinct ozone loss that coincide with the increases in NO_x is not present in the very simple nighttime model, and need another explanation. The observed ozone loss must thus be explained either by nighttime reactions that are not included, or by day-time chemistry. The catalytic nitrogen cycle is essentially powerless at night due to the low concentration of atomic oxygen[2]. This highlights the need to include photolysis in the model, even for seasons where night dominates.

[2]The figure actually show some atomic oxygen even at night. This occurs during the solar storm and is the direct effect of EPP.

3.2 MISU-1D

To simulate the ozone depletion of progressively larger solar proton events, a chemical 1D box model, created by Donal Murtagh, is employed. Using detailed radiative transfer and chemical reaction rate data, the model calculates the diurnal variation of ozone and 20 other compounds in the middle atmosphere. A total of 120 of the most important gas-phase reactions in the middle atmosphere are included, with kinetic parameters specified according to the JPL 2009, except reactions involving HOCl, HO_2 and HCl, which have been updated to JPL 2011. Ozone absorption cross sections are treated according to the 1986 recommendations of the World Meteorological Organization, and employs the algorithm developed by Koppers and Murtagh in 1996 for oxygen absorption cross sections in the Schumann-Runge bands. The Herzberg continuum is derived from the work of Nicolet and Kennes (1986). Multiple scattering and albedo effects are based on the methods described by Meier et al. in 1982. The model aknowledges the sphericity of the Earth by allowing a non-zero transmitted flux for solar zenith angles greater than 90 degrees.Seasonal variations in the earth-sun distance are accounted for, but variability in the solar flux due to the 11 year solar cycle is not included. The differential equations are formed as the sum of the product and loss terms. As these terms ranges over several orders of magnitude, the resulting system is stiff, and must be treated with care. Here, the Shampine and Reichelt (1997)[38] algorithm is employed. For a more comprehensive description of the model, see Khosravi et al.(2012)[39].

The model starts its simulations at 12:00 local solar time, when the solar zenith angle is minimal. The short-lived species are initialized with zero concentrations, as they are formed quickly in the presence of sunlight. The concentration of long-lived species is taken from measurements or output from other models. For the simulations done in this thesis, the initial data are from a coupled chemistry-climate model (the Canadian Middle Atmosphere Model; CMAM). The CIRA-86 climatology contributes with a monthly temperature.

The nitrogen level of each run is controlled by the NO_y constraint. This constraint allows handpicking the volume mixing ratio of NOy, and using this instead of the output from the CMAM dataset. Normally, the short lived species are initialized with zero concentrations at noon, whereas the long-lived species are taken from the output of other models. In contrast, when the NOy constraint is imposed, the initial NO_y amount is composed entirely of the short lived NO.

Figure 11 shows the normal diurnal variation of O_3,O and NO at different latitudes as calculated by the model.

3.3 SD-WACCM-D

The Whole Atmosphere Community Climate Model (WACCM), is a comprehensive numerical 3D model aiming to include fully coupled dynamics and chemistry. It is a grid model with an Eulerian view, and spans altitudes ranging from the ground and up to 140km. The model is frequently updated to include state-of-the-art chemistry, and Gettelman et al.(2019)[40] offers a detailed description of the latest

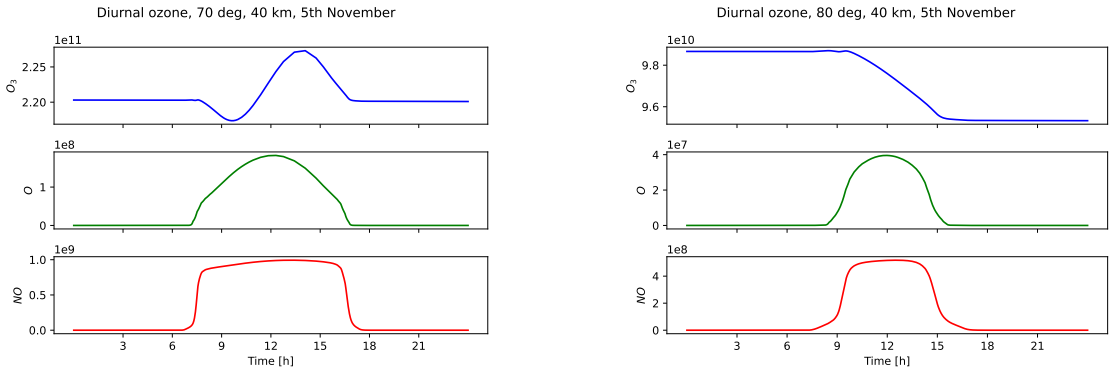

(a) 70 degrees

(b) 80 degrees

Figure 11: Diurnal variation of O3, O, and NO calculated by MISU-1D at 40 km on the 5th of November, the 10th day after initialization.

version, WACCM6.

In order to investigate the chemical response of solar storms, the configuration SD-WACCM-D is used. This version aims to better reproduce the observed effects of Energetic particle precipition(EPP) the D-region of the ionosphere, by incorporating a comprehensive ion chemistry(Verronen et al., 2016)[41].'SD' stands for 'specified dynamics'. At each time step, the horizontal winds and temperatures below 50 km are nudged to follow the meteorological fields of The Modern-Era Retrospective analysis for Research and Applications (MERRA). As this configuration reduces climate noise, as well as wind and temperature biases, the chemical response of events such as SPEs are better reproduced. It should be noted that this configuration decouples the chemistry from the temperature and dynamics in the stratosphere and troposphere, and thus neglects the effect of potential feedback-cycles in these regions.

4 Results and discussions

This section presents the results from using the MISU-1D model to simulate the stratospheric chemistry after progressively larger SPEs. First, there will be a brief presentation of the model settings, before showing the diurnal variation of ozone under different solar zenith angles and amounts of NO_y. The insights given by these plots advocates for the method of creating plots displaying the relationship between ozone depletion and NO_y increases. The plots are then presented, along with a comparison of different latitudes, altitudes and chemistry configurations. Finally, the results are compared with the findings of Kalakoski et al.(2023).

4.1 The diurnal variation of ozone

4.1.1 Model configurations

The MISU-1D model was employed to simulate the stratospheric chemistry for 10 days for different initialization dates, latitudes, and chemistry configuration. As the goal is to see how the ozone loss depends on the increases in NO_y, the NO_y constraint is set to 8 different values; 10, 30, 50, 100, 200, 400, 600 and 800 ppbv. After the initialization day, day 0, each run runs for 10 days. In addition, there is also done a control run with no NO_y constraint for each configuration, that is, one run with the natural amounts of NO_y in the atmosphere. This natural amount depend on latitude, altitude and season. Each run has an altitude grid including 20,25,30,35,40 and 45 km. The initialization dates were chosen to get the same solar conditions and background chemistry as two events previously simulated by SD-WACCM-D; 25th of October 2003 for the Halloween event, and 23rd of July 2012 for Kalakoski et al.'s(2023) hypothetical event.

The model is run for the latitudes 65,70,75,77 and 80 degrees north in October, and for 70N, 80N and 70S in July. This covers the seasons summer, autumn and winter. Additionally, the concentrations of Cl_y, Br_y and H_y($H_y = H_2O + CH_4$) is turned off for one run in July 70N, to isolate the effects that NO_y has on ozone in the absence of other catalytic species.

4.1.2 The diurnal variation of ozone

Three plots depict the diurnal variation of ozone for increasing amounts of NO_y. Figure 12 illustrates the variations at 70 degrees north in October. For low amounts of NO_y, as in the control run, the diurnal variation follows a pattern of decreasing at dusk and dawn, increasing in the middle of the day, and staying fairly constant during the night. Increasing the NO_y amount introduces a couple of new features. Firstly, the ozone decreases faster at dusk; there is a curious drop around four-five in the afternoon. Secondly, as the overall ozone levels decrease, a new rapid increase present itself around 7 in the morning. For the highest amounts of NO_y, the nighttime values drop to zero. For high values of NO_y, it converges towards a curve with two round peaks, one at dawn, and one by the end of midday. All NO_y amounts display ozone increases at midday. The diurnal variation for 70

degrees south, initialized on July 23rd, exhibits similar behavior and is therefore not presented.

Figure 13 also shows the diurnal variation of ozone, but for 80 degrees latitude. For low amounts of NO_y, as seen in the two upper panels, there is a subtle ozone decrease in the middle of the day. The nighttime values are stable. With more NO_y in the atmosphere, the features found at 70 degrees reappear; a rapid increase at dawn, along with a steep drop at dusk. However, with no increase at daytime, the curve looks more like a very flat bell. Additionally, high amounts of NO_y cause nighttime ozone values to drop to zero at 80 degrees as well.

Figure 14 differs from the others, most apparently due to the absence of nighttime. With the atmosphere bathed in sunlight, the curves converge rapidly, even with low amounts of NO_y. However, the control run displays similarities to the control run in 12, as the ozone concentration increases in the middle of the day, and decreases at dusk and dawn. However, dawn follows dusk without a nighttime interlude. For higher NO_y concentrations, the morning minimum is pushed earlier by about two hours. The day time maxima is also reached earlier, and it stays fairly constant during the day.

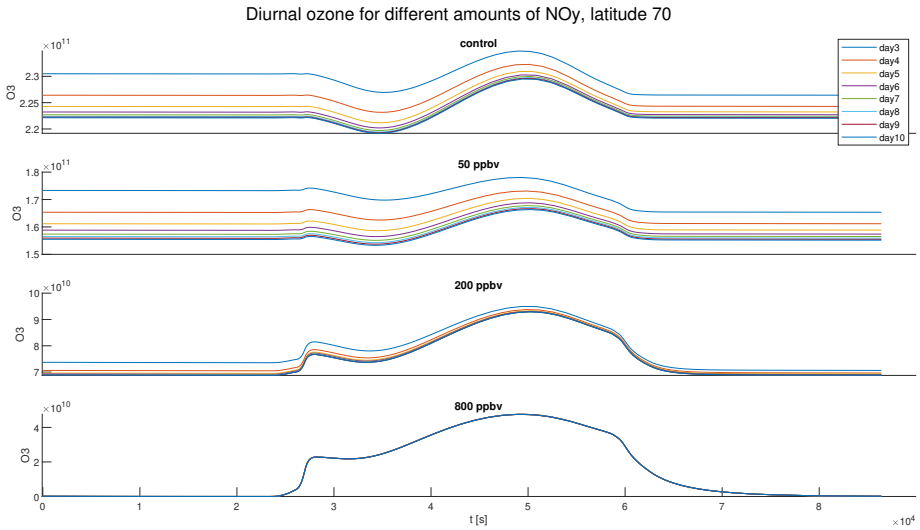

Figure 12: The time evolution of ozone for 10 consecutive days. The simulations are done with the MISU-1D model, and begin 25th October 2003. The first 3 days are omitted for clarity. The four panels represents four different levels of NO_y(control,50,200,800 ppbv), where the control run takes the NO_y value given by the CMAM dataset, and is usually between 10 and 16 ppbv. The altitude is 40 km.

4.1.3 Data analysis choices

The final goal is to create a plot correlating changes in ozone levels with quantities of NO_y. Choosing the ozone concentration relative the control run as the y-axis is a suitable choice, making the results easily comparable to earlier studies, where the results are often presented as a percentage loss. Moreover, if it may be assumed that the real value may be approximated by the modelled value times a scaling

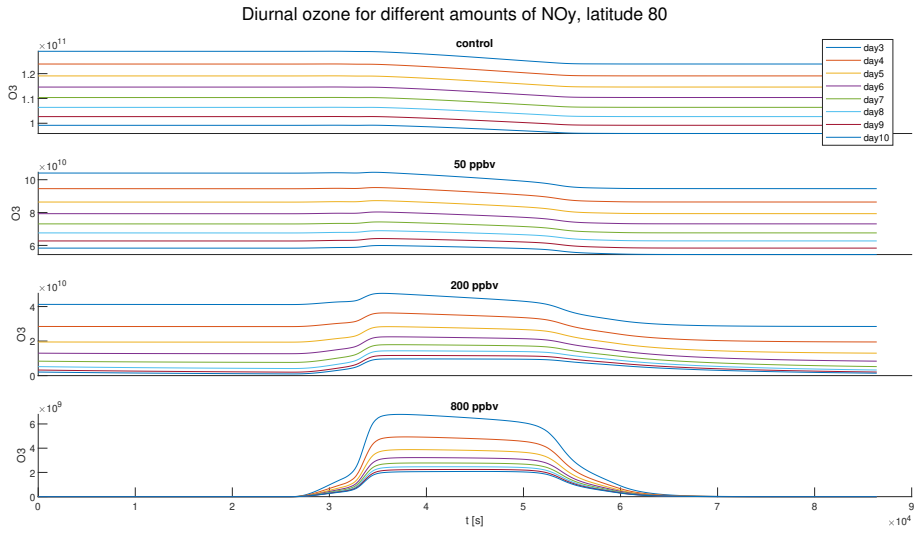

Figure 13: Same as for figure 12 but with latitude 80 instead.

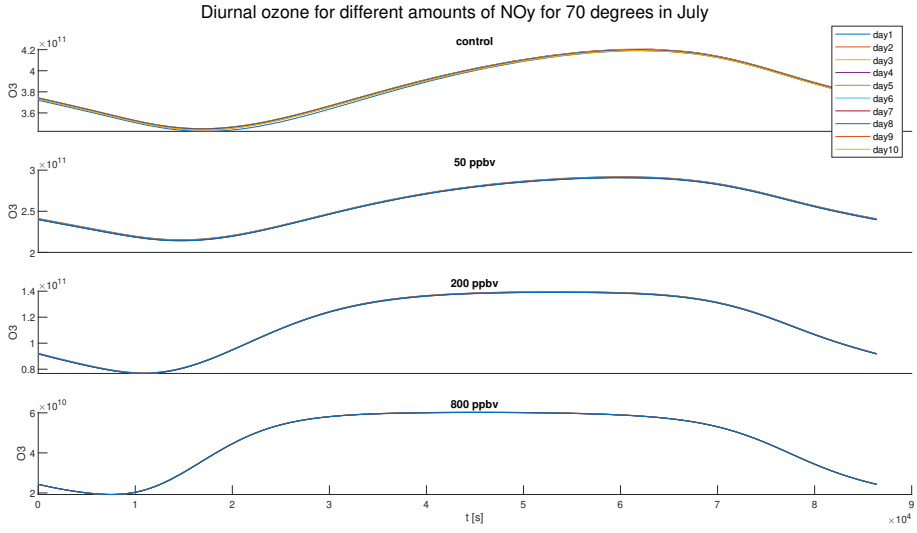

Figure 14: Same as for figure 14 but with July the 23rd as the initialisation date. It converges rapidly, and therefore all days are plotted. The latitude is 70 degrees north.

factor that is unaffected by increases in NO_y, this scaling factor will be cancelled in considering the relative value[3]. The relative value is found by dividing each run with the corresponding control run. There are also several options in choosing the unit for the x-axis, including relative NO_y, volume mixing ratio and number density. The latter perspective would perhaps best illustrate the idea of up-scaling SPEs, assuming odd nitrogen produced is proportional to the particle flux. However, it will vary greatly over altitudes and even latitudes. The NO_y value of the control run at 40 km differs with only about 1 percent between 70 and 80 degrees. At 20 km, this difference between the latitudes increase to 24 percent. Hence, the upcoming results will use relative NO_y as the x-axis, but it should be noted that the control run's concentration may vary across different configurations.

As seen in figures 14 and 13, the ozone value drops to zero at night for high concentrations of NO_y. This is an important result, but it also motivates picking the peak amount of ozone during the day. In the perspective of radiation damage due to ozone loss, it is the day time value that matters. However, should the ozone loss be compared to the loss found by SD-WACCM-D, it would be beneficial to use the concentration averaged over 24 hours[4].

When sunlight is present, the chemical model converges quite rapidly. This motivates picking the ozone value at day 10 as our final value. However, sunlight is scarce at 80N in October, and consequently the model needs more than 10 days to converge, and must thus be treated with caution. If they both overestimate the amount of ozone by the same percentage, this will cancel out in finding the ozone loss relative to the control run. If they overestimate by different factors, the results will not represent the converged state of the chemical model, but rather the ozone loss after ten days of elevated NO_y levels. It is also unreasonable to expect a convergence under changing conditions, with less and less sunlight each passing day.

4.2 Is there a saturation point?

Each plot in the following subsections is generated by fetching the max value of ozone in the 10th day of simulation. This is done for amounts of NO_y ranging from 10 to 800 ppbv, resulting in a curve showing the relationship between ozone depletion and increases in NO_y. It is important to stress that the simulated NO_y amounts in many cases exceeds what is expected after an extreme solar proton event. The simulations presented by Kalakoski et al.(2023) gives an estimate of the relative increases of NO_y for an event comparable to the one 774-775 CE, our

[3]If we assume that there is a real quantity R that we want to model, which is the real impact of NO_y in the atmosphere. We further assume that our modeled value M can be approximately expressed by $M = aR + b$, where a and b are real numbers. Likewise, the control run M_c will be expressed by $M_c = a'R_c + b'$, with the assumption that a' and b' are similar to a and b, as the same model is employed in both cases. We also assume a and b to be independent of the initial increases in NO_y. Choosing the relative value $\frac{M}{M_c}$ is suitable if b is small (the additive noise), but a is significant. The absolute difference value $M - M_c$ gives a more reliable result if a is close to 1, but the additive noise b perturbs the results.

[4]I apologize in advance that this is not done.

current realistic upper bound for solar eruptions. For such an extreme event, the NO_y concentrations could increase with a factor of about 70 at 40 km, and a factor of 6 at 25 km.

Figure 15 displays a curve with relative ozone against relative NO_y. For small increases in NO_y, the ozone drop is drastic, but as expected(Kalakoski et al. 2023, Reddmann et al. 2022), adding more NO_y becomes less effective after a certain point. Increasing the NO_y with a factor of 10 causes an ozone depletion of about 54 percent, whereas a factor of 20 causes a depletion of about 66 percent. The highest factor of NO_y increase that is simulated is 50, moving towards the boundaries of what could reasonably be expected after an extreme solar proton event. In this case, the ozone levels drop to about 20 percent of its natural amount. Could the graph be approximated to any known curve? As a first guess, an exponential fit is attempted in the middle panel, providing a saturation point for ozone of 25 percent. However, several of the data points deviate considerately, and there is not enough evidence to state that a point of saturation exist. Using the logarithm of relative NO_y as the x-axis gives an almost straight line, and a second order polynomial seems to be a good fit. Unfortunately, this function does not provide any insights to the mechanisms underneath, nor does it help in finding a saturation point. A back of the napkin extrapolation reveals that the ozone loss will stagnate first when the NO_y is elevated with a factor of 916, ending up at negative 23 percent relative ozone. This should serve as a warning not to extrapolate, but to treat this solely as a descriptive function.

4.3 Chemistry configurations

Figure 16 shows the effect of including or excluding different chemistry groups from the simulations. At 25 km, there is not much difference between including Cl_y, Br_y and H_y chemistry and not including it. The small horizontal shift between the two curves, with pairs of points side by side, hints at a minor issue with the relative NO_y. This could stem from the fact that the substance $ClONO_2$ is included in both the groups NO_y and Cl_y. If no constraint is imposed, the long lived species are initialized from the CMAM dataset, while imposing the constraint places all the species of the group as short lived species at noon. It is plausible that this method of initialization would include some amount of $ClONO_2$ in one of the control runs, giving origin to the visible shift. This detail should not be given too much attention, as the same result is obtained with and without the shift in NO_y; the model shows that excluding the chemistry groups of Cl_y, Br_y and H_y does not affect the ozone depletion at 25 km.

At 40 km, there is a small effect of excluding these chemistry groups from the model. If all chemistry is included, the ozone loss for the highest amounts of NO_y is 80 percent, compared to a 84 percent loss where the groups are excluded. At a first glance, the right panel gives a contradictory perspective. When the ozone is depicted in number density, it is clear that more ozone is present in an atmosphere without Cl_y, Br_y and H_y, but the ozone loss is greater as well. The leftmost points in the rightmost panel are the values of the control run, the values that the curves

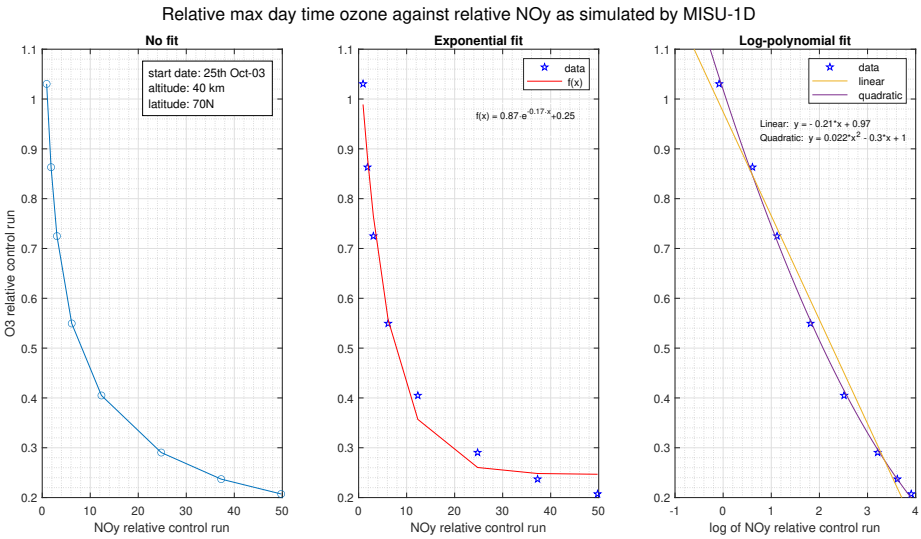

Figure 15: Shows the relative max day time ozone against relative NO_y as simulated by MISU-1D with October 25th 2003 as the date for initialization. The vaules are relative to a control run with natural amounts of NO_y in the atmosphere. The latitude is 70 degrees, and the altitude is 40 km. In the left plot, a weak saturation of ozone loss for high amounts of NO_y can be spotted. The middle panel shows the (failed)attempt of an exponential fit. In the right panel, the ozone loss is plotted against the natural logarithm of relative NO_y, resulting in an approximately linear graph, where a second order polynomial is a good fit. All NO_y values are within what is reasonable to expect for an extreme SPE.

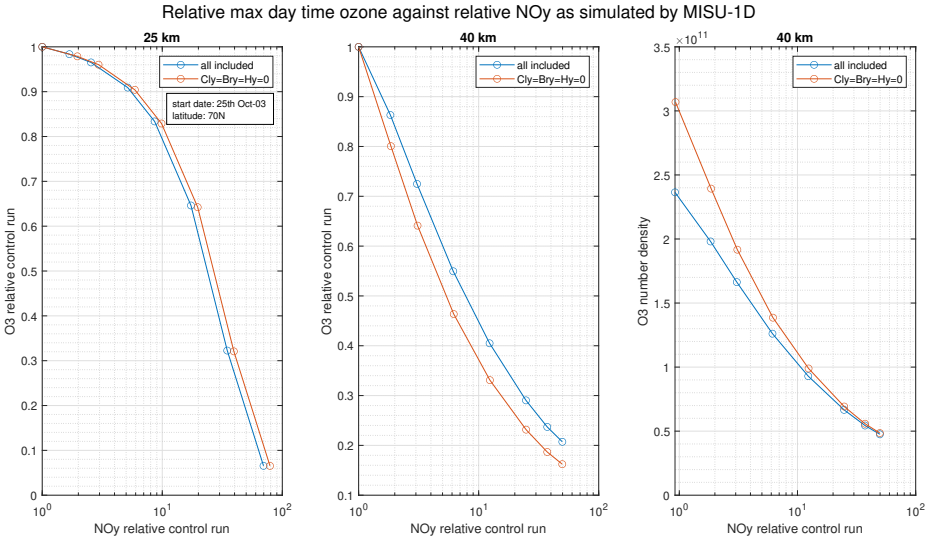

Figure 16: Show the effect of excluding the chemistry groups Cl_y, Br_y and H_y(H_y = H2O + CH4) from the simulations of MISU-1D. The left($z = 20km$) and middle panel($z = 40km$) show the relative max day time ozone against relative NO_y, and the right panel($z = 40km$) display the same data as the middle panel, but as absolute values. October 25th 2003 is the date for initialization, and the latitude is 70N. All NO_y values are within what is reasonable to expect for an extreme SPE.

in the middle panel are divided by. Thus, the observed relative ozone loss at 40 km can be attributed to different background chemistry.

The rightmost panel highlights that the contributions from the excluded chemistry groups matter more for lower amounts of NO_y, but as the NO_y amount increases, the simulation with all chemistry groups included approach the simpler simulation, where they are excluded. Under normal NO_y concentrations, setting Cl_y, Br_y, and H_y to zero would elevate atmospheric ozone levels by diminishing certain ozone loss mechanisms. Nevertheless, aside from reducing ozone, these chemical groups also form reservoir species with NO_x, rendering them unavailable for further reactions. Consequently, these groups act as a buffering mechanism for ozone loss when NO_y concentrations increase, and therefore, an atmosphere without them are more susceptible to severe ozone depletion. From the perspective of the rightmost panel, all active forms of Br_y, Cl_y, and H_y appear to be bound up in reservoir species by NO_y, and the ozone concentration becomes independent of their presence.

It is widely acknowledged that chlorine chemistry can significantly impact ozone levels in the lower stratosphere. The absence of this effect in the model can be attributed to inherent model limitations. The primary cause of effective ozone destruction in the lower stratosphere arises from reactions occurring on the surface of particulates —a reaction scheme not encompassed in the model. In contrast, the typical catalytic destruction by the chlorine or bromine cycle proves more effective in the upper stratosphere(Brasseur et al., 2005)[17].

In conclusion, our analysis indicates that none of the chemical groups Cl_y, Br_y, or H_y significantly alter the results, whether at 25 km or 40 km. Nevertheless, it is imperative to recognize the model's limitations, as it solely captures the effects of gas-phase chemistry, neglecting highly effective surface reactions known to occur in the lower stratosphere. To further explain our results, we redirect our attention away from the Cl_y, Br_y, and H_y groups and center our analysis on the chemistry of nitrogen and oxygen.

4.4 Dependence on latitudes

4.4.1 Different latitudes

How does ozone loss vary with solar zenith angles(SZA)? In October, different latitudes receive varying amounts of sunlight, which impacts the photolysis of atmospheric species. Typically, ozone losses are presented as an average over the polar cap, making it difficult to discern where within the polar cap the majority of ozone loss occurs. Figure 17 illustrates the relative maximum daytime ozone levels against relative NO_y concentrations simulated by MISU-1D. The values are normalized to a control run with natural levels of NO_y in the atmosphere. The altitude considered is 40 km, spanning latitudes from 65 to 80 degrees north. The left panel highlights a significant difference in ozone loss between 70 degrees and 80 degrees north. When NO_y is increased by less than a factor of 5, the ozone loss at 70°N is approximately 5 percent greater than at 80°N. Further increases result in a drastic ozone loss at 80°N, with only a few percent of the ozone remaining if NO_y increases by a factor

of 12.

The right panel displays the curves for five different latitudes: 65, 70, 75, 77, and 80 degrees north. It is noteworthy that the latitudes receiving the most sunlight all exhibit similar curves, showing less ozone depletion than the latitudes receiving less sunlight. This is contrary to expectations, as the catalytic cycles should be more effective during the day.

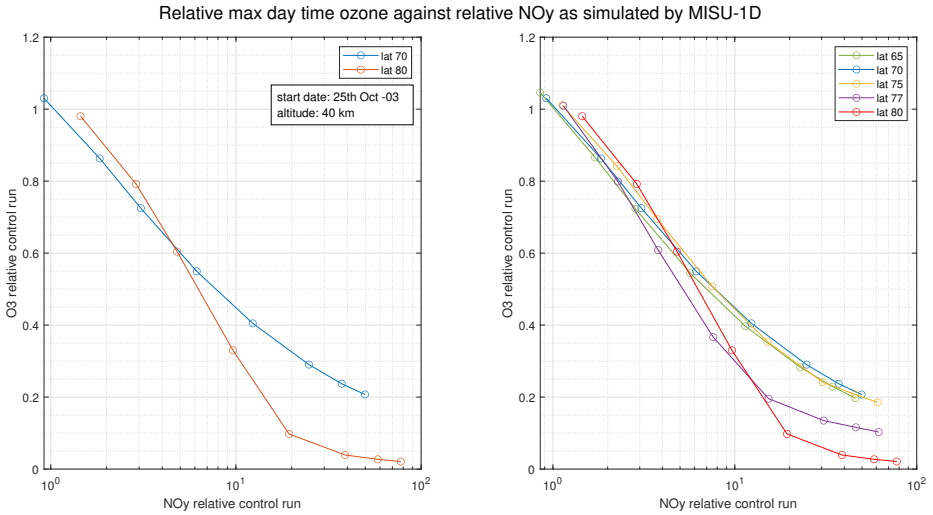

Figure 17: Shows the relative max day time ozone against relative NO_y as simulated by MISU-1D with October 25th 2003 as the date for initialization. The values are relative to a control run with natural amounts of NO_y in the atmosphere. The altitude is 40 km, and the latitudes ranges from 65 to 80 degrees north. The right panel shows all the curves, while the left panels only show 70 and 80 degrees north. Note that the curves for 65,70 and 75 degrees look similar, while 77 and 80 display a more severe ozone loss for large amounts of NO_y.All NO_y values are within what is reasonable to expect for an extreme SPE.

4.4.2 Photolysis and solar zenith angles

The observed differences between 70 and 80 degrees may result from either differences in background chemistry, in solar radiation, or from both. In late October, at 70N, the sun is above the horizon at noon, while at 80N, it is below. As observed in the simple nighttime model, ozone depletion during total nighttime is minimal, as the slow reaction between NO_2 and O_3 is the main contributor. The plots of diurnal ozone witness about the same feature - nightly ozone changes are very small. Therefore, the differences should not be attributed to a greater portion of nighttime.

Figure 18 illustrates solar radiation levels at various latitudes, specifically 70°, 75°, and 80° for an altitude of 40 km. The photolysis of oxygen necessitates wavelengths below 242 nm, but a significant decline in such radiation is evident at 80°, as the sun is below the horizon and the rays travel a longer path. The generation of atomic oxygen is predominantly driven by the photolysis of oxygen, with some contribution from the photolysis of NO_2 and other minor species. As the only path for ozone production is recombination between atomic and molecular oxygen,

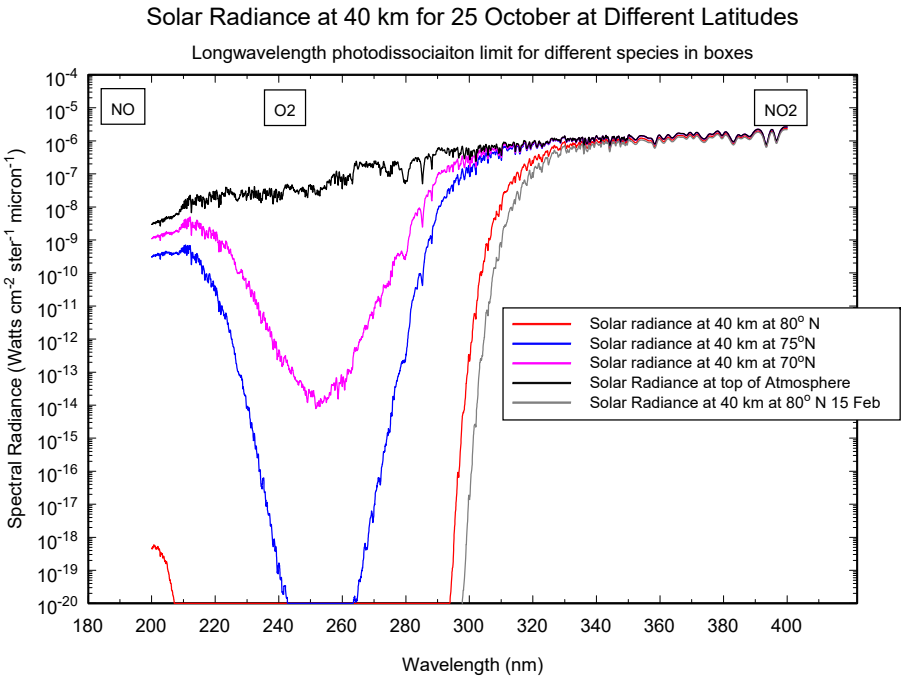

Figure 18: Solar radiance at 40 km for October 25th at noon, for latitudes 70N,75N and 80N. Additionally, the grey curve gives the radiance the 15th of february 80N (same solar conditions as 80S, 23rd of July). Photolysis of NO_2 is possible in all scenarios, meanwhile photolysis of O_2 is only possible for latitudes 70N and 75N.

the sharp decrease in radiation with wavelengths shorter than about 300 nm at 80° results in a lack of ozone production around noon. This agrees well with the diurnal variation in figures 12 and 13, where an ozone increase at noon is present at 70N, but not at 80N.

This radiation cut-off provides a reasonable explanation for a greater ozone loss at 80 degrees than at 70 degrees. However, we have already stated that ozone destruction caused by catalytic nitrogen cycles are more effective in daylight, in the presence of atomic oxygen. However, it should be noted that photolysis of NO_2 occur at both latitudes at noon, which provides a small source of both atomic oxygen and NO, making catalytic destruction possible. This would result in the following reaction scheme at twilight:

$$\mathrm{NO_2} + hv(\lambda < 398nm) \longrightarrow NO + O \tag{40}$$
$$\mathrm{O_3} + hv(\lambda < 320nm) \longrightarrow \mathrm{O_2} + O \tag{41}$$
$$O + \mathrm{O_2} + M \longrightarrow \mathrm{O_3} + M \tag{42}$$
$$\mathrm{NO_2} + O \longrightarrow NO + \mathrm{O_2} \tag{43}$$
$$NO + \mathrm{O_3} \longrightarrow \mathrm{NO_2} + \mathrm{O_2} \tag{44}$$
$$O + \mathrm{O_3} \longrightarrow 2\mathrm{O_2} \tag{45}$$

Equations 40, 41, and 42 display an equilibrium where ozone is both produced and destroyed, providing a small concentration of atomic oxygen. During the daytime, equation 43, which turns NO_2 back into NO, is an important part of the catalytic cycle. However, this reaction weakens at twilight when there is little atomic oxygen. Nevertheless, the photolysis of NO_2 accomplishes the same task. Under these conditions, ozone loss with low amounts of atomic oxygen is possible. The effectiveness of the catalytic cycle at twilight versus in daylight is not quantified. A reasonable guess would be that the destruction is stronger during the day, but that this loss is counteracted by ozone production due to a higher amount of O.

Verronen et al.(2005)[42] made the same observations in their chemical model of the atmosphere during the Halloween storms, of ozone depletion at sunrise and sunset, and ozone recovery at noon and afternoon. Their modelling is comparable to the model in this study, as they used a one-dimensional ion and neutral chemistry model, initialized the model on 26th October 2003, and used 70N as the latitude, leading to almost identical solar conditions.

4.4.3 Different latitudes and altitudes

Figure 19 shows how the ozone saturation depend on altitudes for the latitudes 70, 75 and 80 degrees. The plots for 70 and 75 degrees look similar, while the one for 80 is the odd one out, as was found in the previous section. The altitudes of 20 and 25 km has a qualitatively different behaviour than the higher altitudes. All latitudes show very little ozone loss for 20 km. For 70 degrees and at 20 km, a 100-fold increase in NO_y cause a ozone decrease of less than 2 percent. At 80N, the altitudes 35,40 and 45 km all follow the same curve, giving a more serious ozone loss. In contrast, the ozone loss at 20 and 25 km is more modest at this latitude, than further south. It must also be taken into account that for altitudes lower than about 35 km, such a large increase in NO_y becomes increasingly hypothetical, and does not reproduce what would have occurred during an actual solar proton event. These differences may have a number of potential sources, as the chemistry at 40 km differ significantly from that at 20 km, especially in considering the amount of atomic oxygen at daytime.

We see that the trend of more ozone depletion at 80N holds in the upper stratosphere. But there is also a small difference between 70N and 75N at 35 km, where the latter experience a higher degree of loss. As the sun is above the horizon, the rays illuminating the atmosphere at 35km has a longer path, and it is possible that the photolysis of oxygen at noon is very diminished, causing the same behaviour as was seen for 80N at 40km. Perhaps this is also the reason for the ozone loss seen at 30 km for 70N. However, this is merely a speculation, and not confirmed by solar radiation data. The rightmost plot, at 80N, shows a peculiar feature, with a clear distinction between the lower stratosphere (20-25km), and the upper stratosphere(30-45km). A possible explanation could be that photolysis of NO_2, and thus the possibility of catalytic destruction, is only present at higher altitudes. The semilog axis also hides the fact that the curves of 20 and 25 km is very close to being linear. This would be the expected shape at night, where the recombination

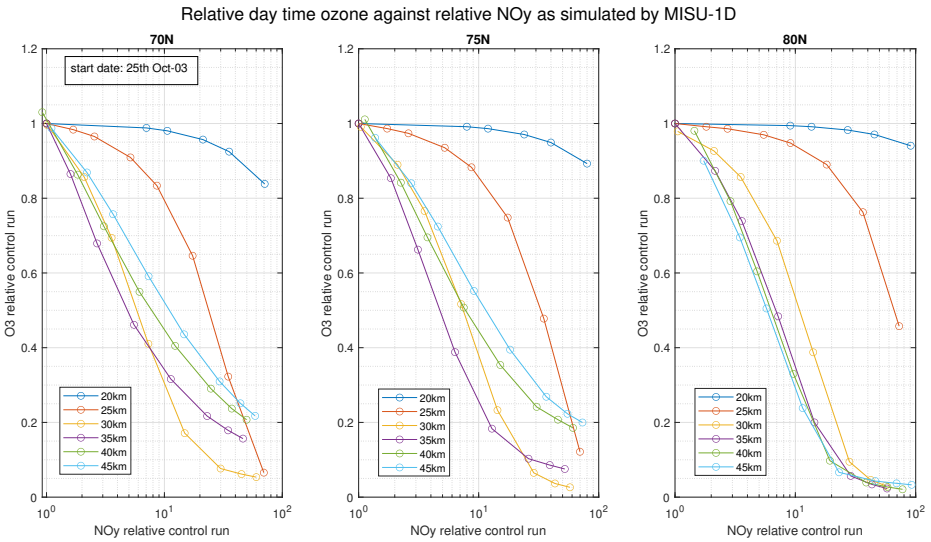

Figure 19: Shows the relative max day time ozone against relative NO_y as simulated by MISU-1D with October 25th 2003 as the date for initialization. The three panels show the latitudes 70,75 and 80 degrees north, from left to right. The values are relative to a control run with natural amounts of NO_y in the atmosphere. The latitude is 70N, and the altitudes ranges from 20 to 45km. It should be noted that for an extreme SPE, the NO_y can be expected to increase by a factor of about 70 at 40 km, and with a factor of 7 at 25 km. Consequently, some of the curves stretches into the hypothetical realm.

between NO_2 and O_3 is the dominant source of ozone loss.

4.5 Comparing models

In 2012 there was a solar storm of the same magnitude as the Halloween storms, that barely missed planet Earth. Fortunately, the ionization was recorded by the satellite STEREO. Kalakoski et al.(2023) used this ionization data to simulate with SD-WACCM-D what the atmospheric impact would have been had the solar storm been pitched directly at the earth. Additionally, the simulations was done with ionization scaled up by 10 and 100. Multiplying with 100 would result in a solar storm of about the same magnitude as the 774-775 AD storms, our current upper bound of solar storm severity. The data is a polar cap weighted area, and averaged over 24 hours. See Kalakoski et al.(2023) for a more comprehensive explanation of the data simulation. To get a reasonable method of comparing these results with the results from MISU-1D, we are looking at the ozone loss that coincide with an elevated level of NO_y caused by the ionization. Thus, we are looking at the indirect effects, as the maximum amount of NO_y in the stratosphere may occur weeks after the event due to downwelling. Figure 20 show a comparison between the results from SD-WACCM-D and the results from the MISU-1D. Because the SD-WACCM-D-simulated solar storm occurred in July, and show results from both hemispheres, the initialization date for the MISU-1D was set to July 23rd for both the NH and the SH. Thus the results from SD-WACCM-D are compared with the MISU-1D results from three different seasons: summer, autumn and winter.

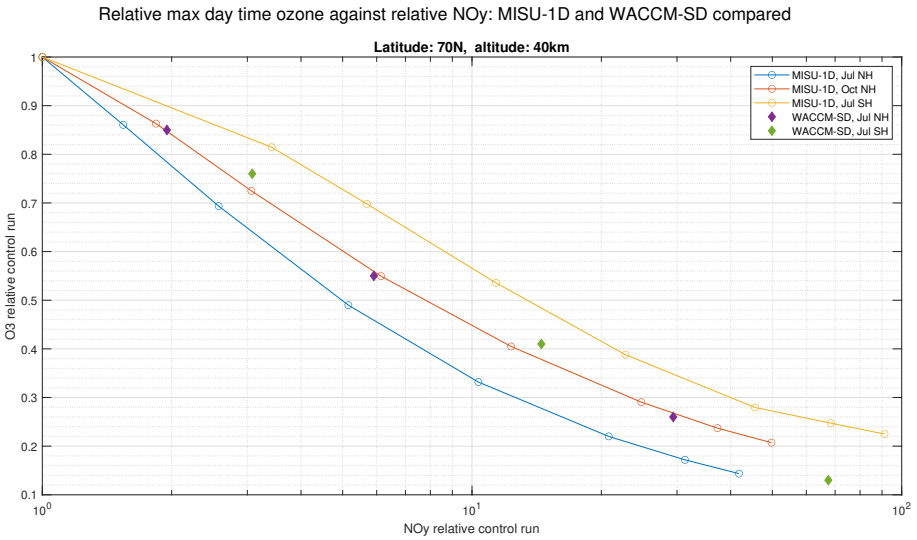

Figure 20: Shows the relative max day time ozone against relative NO_y as simulated by MISU-1D and SD-WACCM-D for two different dates of initialization: October 25th 2003, and July 23rd 2012 at both hemispheres. 23rd July in the SH gives the same solar conditions as 15th February in the NH. The values are relative to a control run with natural amounts of NO_y in the atmosphere. The altitude is 40 km, and the latitude is 70 degrees for both hemispheres. All values of NO_y are whitin what is expected after an extreme SPE.

There is a surprisingly good agreement between the SD-WACCM-D and the October runs at 70 degrees latitude. However, the SD-WACCM-D simulations should be expected to agree better with the runs initialized in July, and not in October. When the MISU-1D is compared directly to July, it underestimates the loss, and when compared to July SH, the loss is overestimates. The main difference between the two models are the inclusion of transport that alters the background level of NO_y. Due to the Brewer-Dobson circulation, the month of July exhibit upwelling in the NH, and downwelling in the SH. Late October in the NH has only a weak downwelling. Due to the rather neutral vertical transport of October, the exclusion of dynamics in the MISU-1D would cause fewer discrepancies this month.

Two other factors could be crucial for the results. Firstly, the two models could be operating at quite different temperatures, as the MISU-1D uses a monthly mean temperature, and use the same temperature for day and night, whereas SD-WACCM-D operates with temperatures that are updated more frequently. Some of the rate coefficients depend heavily on temperature, and a higher/lower temperature would push the reactions in the direction of more/less ozone(CHECK THIS!!!!!). Secondly, the two models may have a very different background chemistry, and thus looking at the relative amount of NO_y and O_3 might not be the best way to compare the two models. Figure 21 show two different ways of viewing the ozone loss of the three seasons: by absolute amounts or by relative amounts. These two views give the opposite impression of what season causes the most ozone loss. The left panel(relative amounts) gives the impression of ozone loss being most severe in the summer, but the right panel reveals that the enormous relative loss is

due to a very high ozone concentration in the control run. In July, a factor of 10 differ the NH from the SH. Such a high value is the result of 10 consecutive days of sunlight with no transport mechanism to serve as an ozone sink.

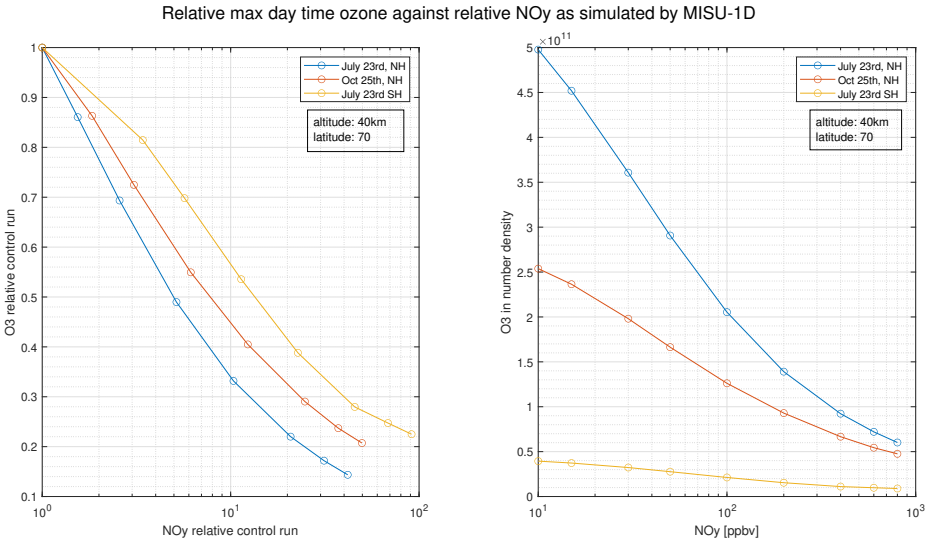

Figure 21: Shows the relative max day time ozone against relative NO_y as simulated by MISU-1D for two different dates of initialization: October 25th 2003 and July 23rd 2012 at both hemispheres. 23rd July in the SH gives the same solar conditions as 15th February in the NH. The values are relative to a control run with natural amounts of NO_y in the atmosphere. The altitude is 40 km, and the latitude is 70 degrees for both hemispheres. All values of NO_y are whitin what is expected after an extreme SPE.

Figure 22 is similar to 20, but with absolute differences instead of relative values. With this method, none of the curves simulated by MISU-1D are a good match to SD-WACCM-D. The curve for July is the closest match; it agrees well for low values of NO_y, but the concentration of ozone deviates with about 1 ppmv when the NO_y concentration approach 1 ppmv. The catalytic nitrogen cycles are the primary drivers behind the ozone loss. In daylight, there is a partitioning between O and O_3, such that O is proportional to O_3. Consequently, the rates of both these equations are proportional with ozone, making it reasonable to expect a better agreement when percentages are used, rather than absolute values.

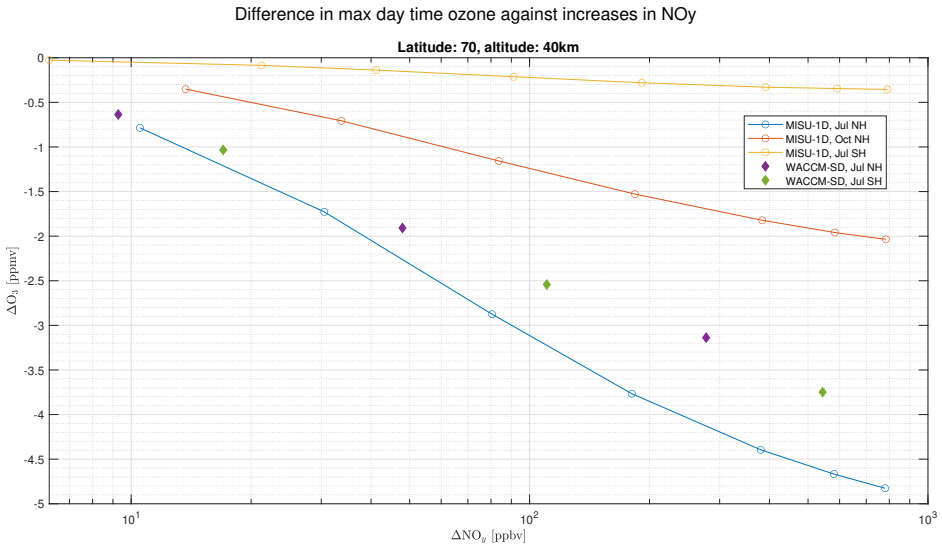

Figure 22: Same as for figure 20, but with absolute differences instead of relative values.

5 Conclusions

In the aftermath of very large solar proton events, the stratosphere experience elevated amounts of NO_y and HO_y. Both of these chemistry groups has a significant effect on ozone, as they are involved in catalytic ozone destruction. NO_y has a long life-time, and may therefore perturb the atmosphere for weeks or months after the ionization occurred. The associated ozone loss for solar proton events of moderate magnitudes are well documented, but the impacts of extreme and rare events relies heavily on model predictions. This study explores the chemical impacts of such events on the stratospheric ozone, with the use of a MISU-1D, a chemical box model. By simulating the ozone loss under increasing amounts of NO_y, two questions of interest was addressed. Firstly, the severity of extreme amounts of stratospheric NO_y was assessed, with the aim to search for a saturation point where adding more NO_y caused no further ozone loss. Secondly, by employing a purely chemical model, the causes behind the ozone loss was examined.

As a first step, a very simple nighttime model was created, including only oxygen and nitrogen species. The results at 40 km altitude did not agree well with data from the Halloween event in 2003 as simulated by SD-WACCM-D. The lack of ozone loss in the nighttime model was attributed to the neglection of photolysis. With no source of atomic oxygen, the catalytic nitrogen cycles are powerless. This emphasized the crucial role of photolysis, even for seasons and latitudes dominated by night. Therefore, MISU-1D was employed, a comprehensive chemical box model that calculates the diurnal variation of 21 species in the middle atmosphere.

MISU-1D simulated the ozone concentrations in an atmosphere with amounts of NO_y ranging from 10 ppbv to 800 ppbv. At an altitude of 40 km, a latitude of 70N, and a NO_y amount of 800 ppbv, the diurnal variation of ozone displayed an almost complete ozone destruction at night, but a peak number density of about $5 * 10^{10}/cm^3$ after noon. The same result is found at 80N, although with a more severe ozone loss. The ozone concentration increases during daytime, decreases during twilight, and stays fairly constant throughout the night.

At 40 km altitude, and 70 degrees north, there was no evidence of a saturation point, where ozone is unaffected by a further increase in NO_y. However, about 50 percent of the ozone was already depleted with a 9-fold increase in NO_y, and 20 percent remained under a 50-fold increase. The curve was well described by the descriptive function

$$O_{3,rel} = 0.022log(NO_{y,rel})^2 - 0.3log(NO_{y,rel}) + 1, \tag{46}$$

where O_3 and NO_y are both relative to the control run.

The effects of removing the chemistry groups of Cly, Bry, H2O and CH4 from the model was insignificant at 25 km, and altered the results by only a few percent at 40km.

The ozone loss proved to depend on latitudes. The curves for 65,70 and 75 were

similar, whereas the ones for 77 and 80 differed, with a more severe ozone loss. This difference was attributed to the lack of photolysis of oxygen at noon at 80N, causing less ozone to be produced. At twilight, the photolysis of NO2 makes catalytic cycles possible. At 80N there is enough sunlight to catalytically destroy ozone, but not enough to produce ozone via photolysis of oxygen. The destruction depend on altitudes as well, and the ozone loss is more severe in the upper stratosphere than in the lower.

The results of MISU-1D from three different seasons, summer, autumn and winter, gives diverging results, with a seemingly more efficient ozone depletion in the summer than in the winter, with the autumn in between. Although the ozone loss in July seem drastic when relative amounts are considered, this is due to a higher ozone concentration in the control run. There is a decent agreement between the results from MISU-1D and the SD-WACCM-D simulations done by Kalakoski et al.(2023). The simulation of July NH overestimates the loss by about 10 percent, July SH underestimates by the same amount, while the curve for October is very good match. A possible explanation is the up- and down-welling in July, compared to the relatively stable vertical dynamics of October. The relative amount is a better mode for comparing the two models than the absolute amounts, as the rate for the catalytic nitrogen cycles are proportional to O3, so in the relative case, the background difference in ozone is cancelled out. The sensitivity to temperature is not explored. MISU-1D has several limitations, and although the calculated diurnal variation has been showed to be in well agreement with observations at low latitudes, the model is not yet verified for the polar latitudes. Moreover, the lack of surface phase chemistry makes the results in the lower stratosphere unreliable.

The correlation between NO_y increases and decreases in O_3 is a quick tool for estimating the ozone loss after a SPE without simulating it. Additionally, it may contribute in the aim to correctly parameterize the relation between EPP and ozone in climate models.

References

[1] Charles H. Jackman, Richard D. McPeters, Gordon J. Labow, Eric L. Fleming, Cid J. Praderas, and James M. Russell. Northern hemisphere atmospheric effects due to the july 2000 solar proton event. *Geophysical Research Letters*, 28(15):2883–2886, 2001. doi: https://doi.org/10.1029/2001GL013221. URL `https://agupubs.onlinelibrary.wiley.com/doi/abs/10.1029/2001GL013221`.

[2] C. H. Jackman, D. R. Marsh, F. M. Vitt, R. R. Garcia, E. L. Fleming, G. J. Labow, C. E. Randall, M. López-Puertas, B. Funke, T. von Clarmann, and G. P. Stiller. Short- and medium-term atmospheric constituent effects of very large solar proton events. *Atmospheric Chemistry and Physics*, 8(3):765–785, 2008. doi: 10.5194/acp-8-765-2008. URL `https://acp.copernicus.org/articles/8/765/2008/`.

[3] Craig J. Rodger, Pekka T. Verronen, Mark A. Clilverd, Annika Seppälä, and Esa Turunen. Atmospheric impact of the carrington event solar protons. *Journal of Geophysical Research: Atmospheres*, 113(D23), 2008. doi: https://doi.org/10.1029/2008JD010702. URL `https://agupubs.onlinelibrary.wiley.com/doi/abs/10.1029/2008JD010702`.

[4] M. Calisto, P. T. Verronen, E. Rozanov, and T. Peter. Influence of a carrington-like event on the atmospheric chemistry, temperature and dynamics. *Atmospheric Chemistry and Physics*, 12(18):8679–8686, 2012. doi: 10.5194/acp-12-8679-2012. URL `https://acp.copernicus.org/articles/12/8679/2012/`.

[5] G. Rohen, C. von Savigny, M. Sinnhuber, E. J. Llewellyn, J. W. Kaiser, C. H. Jackman, M.-B. Kallenrode, J. Schröter, K.-U. Eichmann, H. Bovensmann, and J. P. Burrows. Ozone depletion during the solar proton events of october/november 2003 as seen by sciamachy. *Journal of Geophysical Research: Space Physics*, 110(A9), 2005. doi: https://doi.org/10.1029/2004JA010984. URL `https://agupubs.onlinelibrary.wiley.com/doi/abs/10.1029/2004JA010984`.

[6] M. E. Andersson, P. T. Verronen, D. R. Marsh, S.-M. Päivärinta, and J. M. C. Plane. Waccm-d—improved modeling of nitric acid and active chlorine during energetic particle precipitation. *Journal of Geophysical Research: Atmospheres*, 121(17):10,328–10,341, 2016. doi: https://doi.org/10.1002/2015JD024173. URL `https://agupubs.onlinelibrary.wiley.com/doi/abs/10.1002/2015JD024173`.

[7] T. Sukhodolov, I. Usoskin, and E. Rozanov et al. Atmospheric impacts of the strongest known solar particle storm of 775 ad. *Sci Rep*, 7, 2017. doi: https://doi.org/10.1038/srep45257.

[8] T. Reddmann, M. Sinnhuber, J. M. Wissing, O. Yakovchuk, and I. Usoskin. The impact of a solar extreme event on the middle atmosphere, a case study. *Atmospheric Chemistry and Physics Discussions*, 2023:1–21, 2023.

doi: 10.5194/acp-2023-31. URL https://acp.copernicus.org/preprints/acp-2023-31/.

[9] N. Kalakoski, P.T. Verronen, and M.E. et al. Szeląg. Global ozone loss following extreme solar proton storms based on the july 2012 coronal mass ejection. *Sci Rep 13*, page 13873, 2023. doi: https://doi.org/10.1038/s41598-023-40129-1.

[10] David G. Andrews. *An introduction to atmospheric physics*. Cambridge University Press, 2010. doi: https://doi.org/10.1017/CBO9780511800788.

[11] I. I. Baliukin, J.-L. Bertaux, E. Quémerais, V. V. Izmodenov, and W. Schmidt. Swan/soho lyman-α mapping: The hydrogen geocorona extends well beyond the moon. *Journal of Geophysical Research: Space Physics*, 124(2):861–885, 2019. doi: https://doi.org/10.1029/2018JA026136. URL https://agupubs.onlinelibrary.wiley.com/doi/abs/10.1029/2018JA026136.

[12] Gordon Miller Bourne Dobson, D. N. Harrison, and J. Lawrence. Measurements of the amount of ozone in the earth's atmosphere and its relation to other geophysical conditions.—part iii. *Proceedings of the Royal Society of London. Series A, Containing Papers of a Mathematical and Physical Character*, 122(790):456–486, 1929. doi: 10.1098/rspa.1929.0034. URL https://royalsocietypublishing.org/doi/abs/10.1098/rspa.1929.0034.

[13] A. W. Brewer. Evidence for a world circulation provided by the measurements of helium and water vapour distribution in the stratosphere. *Quarterly Journal of the Royal Meteorological Society*, 75(326):351–363, 1949. doi: https://doi.org/10.1002/qj.49707532603. URL https://rmets.onlinelibrary.wiley.com/doi/abs/10.1002/qj.49707532603.

[14] Neal Butchart. The brewer-dobson circulation. *Reviews of Geophysics*, 52 (2):157–184, 2014. doi: https://doi.org/10.1002/2013RG000448. URL https://agupubs.onlinelibrary.wiley.com/doi/abs/10.1002/2013RG000448.

[15] Timothy Dunkerton. On the mean meridional mass motions of the stratosphere and mesosphere. *Journal of Atmospheric Sciences*, 35(12):2325 – 2333, 1978. doi: https://doi.org/10.1175/1520-0469(1978)035<2325:OTMMMM>2.0.CO;2. URL https://journals.ametsoc.org/view/journals/atsc/35/12/1520-0469_1978_035_2325_otmmmm_2_0_co_2.xml.

[16] H. Bönisch, A. Engel, Th. Birner, P. Hoor, D. W. Tarasick, and E. A. Ray. On the structural changes in the brewer-dobson circulation after 2000. *Atmospheric Chemistry and Physics*, 11(8):3937–3948, 2011. doi: 10.5194/acp-11-3937-2011. URL https://acp.copernicus.org/articles/11/3937/2011/.

[17] Guy P. Brasseur and Susan Solomon. *Composition and Chemistry*, pages 265–442. Springer Netherlands, Dordrecht, 2005. ISBN 978-1-4020-3824-2. doi: 10.1007/1-4020-3824-0_5. URL https://doi.org/10.1007/1-4020-3824-0_5.

[18] Rolando R Garcia and Susan Solomon. The effect of breaking gravity waves on the dynamics and chemical composition of the mesosphere and lower ther-

mosphere. *Journal of Geophysical Research: Atmospheres*, 90(D2):3850–3868, 1985.

[19] J. Farman, B. Gardiner, and J. Shanklin. Large losses of total ozone in antarctica reveal seasonal clox/nox interaction. *Nature*, 315:207–210, 1985. doi: https://doi.org/10.1038/315207a0.

[20] Mario J. Molina. Polar ozone depletion (nobel lecture). *Angewandte Chemie International Edition in English*, 35(16):1778–1785, 1996. doi: https://doi.org/10.1002/anie.199617781. URL `https://onlinelibrary.wiley.com/doi/abs/10.1002/anie.199617781`.

[21] National Aeronautics and Space Administration. NASA Ozone Watch. `https://ozonewatch.gsfc.nasa.gov/`, n.d. Accessed: January 8, 2024.

[22] Simchan Yook, David W. J. Thompson, and Susan Solomon. Climate impacts and potential drivers of the unprecedented antarctic ozone holes of 2020 and 2021. *Geophysical Research Letters*, 49(10):e2022GL098064, 2022. doi: https://doi.org/10.1029/2022GL098064. URL `https://agupubs.onlinelibrary.wiley.com/doi/abs/10.1029/2022GL098064`. e2022GL098064 2022GL098064.

[23] T. Egorova, J. Sedlacek, T. Sukhodolov, A. Karagodin-Doyennel, F. Zilker, and E. Rozanov. Montreal protocol's impact on the ozone layer and climate. *Atmospheric Chemistry and Physics*, 23(9):5135–5147, 2023. doi: 10.5194/acp-23-5135-2023. URL `https://acp.copernicus.org/articles/23/5135/2023/`.

[24] V.E. Fioletov. Ozone climatology, trends, and substances that control ozone. *Atmosphere-Ocean*, 46(1):39–67, 2008. doi: 10.3137/ao.460103. URL `https://doi.org/10.3137/ao.460103`.

[25] Takatoshi Sakazaki, Masatomo Fujiwara, Chihiro Mitsuda, Koji Imai, Naohiro Manago, Yoko Naito, Tetsu Nakamura, Hideharu Akiyoshi, Douglas Kinnison, Takuki Sano, Makoto Suzuki, and Masato Shiotani. Diurnal ozone variations in the stratosphere revealed in observations from the superconducting submillimeter-wave limb-emission sounder (smiles) on board the international space station (iss). *Journal of Geophysical Research: Atmospheres*, 118 (7):2991–3006, 2013. doi: https://doi.org/10.1002/jgrd.50220. URL `https://agupubs.onlinelibrary.wiley.com/doi/abs/10.1002/jgrd.50220`.

[26] Kenneth R Lang. *The Sun from space*. Springer Science & Business Media, 2008.

[27] Dermott J Mullan. *Physics of the Sun: A first course*. CRC press, 2010.

[28] M.A. Shea and D.F. Smart. Space weather and the ground-level solar proton events of the 23rd solar cycle. *Space Sci Rev*, 171:161–188, 2012. doi: 10.1007/s11214-012-9923-z.

[29] Syun-Ichi Akasofu. A historical review of the geomagnetic storm-producing plasma flows from the sun. *Space science reviews*, 164:85–132, 2011.

[30] Qiuzhen Zhong, Jingjing Wang, Xuejie Meng, Siqing Liu, and Jiancun Gong. Prediction model for solar energetic proton events: Analysis and verification. *Space Weather*, 17(5):709–726, 2019. doi: https://doi.org/10.1029/2018SW001915. URL https://agupubs.onlinelibrary.wiley.com/doi/abs/10.1029/2018SW001915.

[31] H. Nesse Tyssøy and J. Stadsnes. Cutoff latitude variation during solar proton events: Causes and consequences. *Journal of Geophysical Research: Space Physics*, 120(1):553–563, 2015. doi: https://doi.org/10.1002/2014JA020508. URL https://agupubs.onlinelibrary.wiley.com/doi/abs/10.1002/2014JA020508.

[32] Daniel N. Baker, Glenn M. Mason, and Joseph E. Mazur. A small spacecraft mission with large accomplishments. *Eos, Transactions American Geophysical Union*, 93(34):325–326, 2012. doi: https://doi.org/10.1029/2012EO340001. URL https://agupubs.onlinelibrary.wiley.com/doi/abs/10.1029/2012EO340001.

[33] Irina A Mironova, Karen L Aplin, Frank Arnold, Galina A Bazilevskaya, R Giles Harrison, Alexei A Krivolutsky, Keri A Nicoll, Eugene V Rozanov, Esa Turunen, and Ilya G Usoskin. Energetic particle influence on the earth's atmosphere. *Space science reviews*, 194:1–96, 2015.

[34] HS Porter, CH Jackman, and AES Green. Efficiencies for production of atomic nitrogen and oxygen by relativistic proton impact in air. *The Journal of Chemical Physics*, 65(1):154–167, 1976.

[35] S. Solomon, D.W. Rusch, J.C. Gérard, G.C. Reid, and P.J. Crutzen. The effect of particle precipitation events on the neutral and ion chemistry of the middle atmosphere: Ii. odd hydrogen. *Planetary and Space Science*, 29(8):885–893, 1981. ISSN 0032-0633. doi: https://doi.org/10.1016/0032-0633(81)90078-7. URL https://www.sciencedirect.com/science/article/pii/0032063381900787.

[36] Beatriz Sánchez-Cano, Olivier Witasse, Elise W. Knutsen, Dikshita Meggi, Shayla Viet, Mark Lester, Robert F. Wimmer-Schweingruber, Marco Pinto, Richard Moissl, Johannes Benkhoff, Hermann Opgenoorth, Uli Auster, Jos de Brujine, Peter Collins, Guido De Marchi, David Fischer, Yoshifumi Futaana, James Godfrey, Daniel Heyner, Mats Holmstrom, Andrew Johnstone, Simon Joyce, Daniel Lakey, Santa Martinez, David Milligan, Elsa Montagnon, Daniel Müller, Stefano A. Livi, Timo Prusti, Jim Raines, Ingo Richter, Daniel Schmid, Peter Schmitz, Håkan Svedhem, Matt G. G. T. Taylor, Elena Tremolizzo, Dimitri Titov, Colin Wilson, Simon Wood, and Joe Zender. Solar energetic particle events detected in the housekeeping data of the european space agency's spacecraft flotilla in the solar system. *Space Weather*, 21(8):e2023SW003540, 2023. doi: https://doi.org/10.1029/

2023SW003540. URL https://agupubs.onlinelibrary.wiley.com/doi/abs/10.1029/2023SW003540. e2023SW003540 2023SW003540.

[37] J. Jia, A. Kero, N. Kalakoski, M. E. Szeląg, and P. T. Verronen. Is there a direct solar proton impact on lower-stratospheric ozone? *Atmospheric Chemistry and Physics*, 20(23):14969–14982, 2020. doi: 10.5194/acp-20-14969-2020. URL https://acp.copernicus.org/articles/20/14969/2020/.

[38] Lawrence F Shampine and Mark W Reichelt. The matlab ode suite. *SIAM journal on scientific computing*, 18(1):1–22, 1997.

[39] Maryam Khosravi. *Diurnal variation of stratospheric short-lived species*. Chalmers Tekniska Hogskola (Sweden), 2012.

[40] A. Gettelman, M. J. Mills, D. E. Kinnison, R. R. Garcia, A. K. Smith, D. R. Marsh, S. Tilmes, F. Vitt, C. G. Bardeen, J. McInerny, H.-L. Liu, S. C. Solomon, L. M. Polvani, L. K. Emmons, J.-F. Lamarque, J. H. Richter, A. S. Glanville, J. T. Bacmeister, A. S. Phillips, R. B. Neale, I. R. Simpson, A. K. DuVivier, A. Hodzic, and W. J. Randel. The whole atmosphere community climate model version 6 (waccm6). *Journal of Geophysical Research: Atmospheres*, 124(23):12380–12403, 2019. doi: https://doi.org/10.1029/2019JD030943. URL https://agupubs.onlinelibrary.wiley.com/doi/abs/10.1029/2019JD030943.

[41] P. T. Verronen, M. E. Andersson, D. R. Marsh, T. Kovács, and J. M. C. Plane. Waccm-d—whole atmosphere community climate model with d-region ion chemistry. *Journal of Advances in Modeling Earth Systems*, 8(2):954–975, 2016. doi: https://doi.org/10.1002/2015MS000592. URL https://agupubs.onlinelibrary.wiley.com/doi/abs/10.1002/2015MS000592.

[42] Pekka T. Verronen, Annika Seppälä, Mark A. Clilverd, Craig J. Rodger, Erkki Kyrölä, Carl-Fredrik Enell, Thomas Ulich, and Esa Turunen. Diurnal variation of ozone depletion during the october–november 2003 solar proton events. *Journal of Geophysical Research: Space Physics*, 110(A9), 2005. doi: https://doi.org/10.1029/2004JA010932. URL https://agupubs.onlinelibrary.wiley.com/doi/abs/10.1029/2004JA010932.

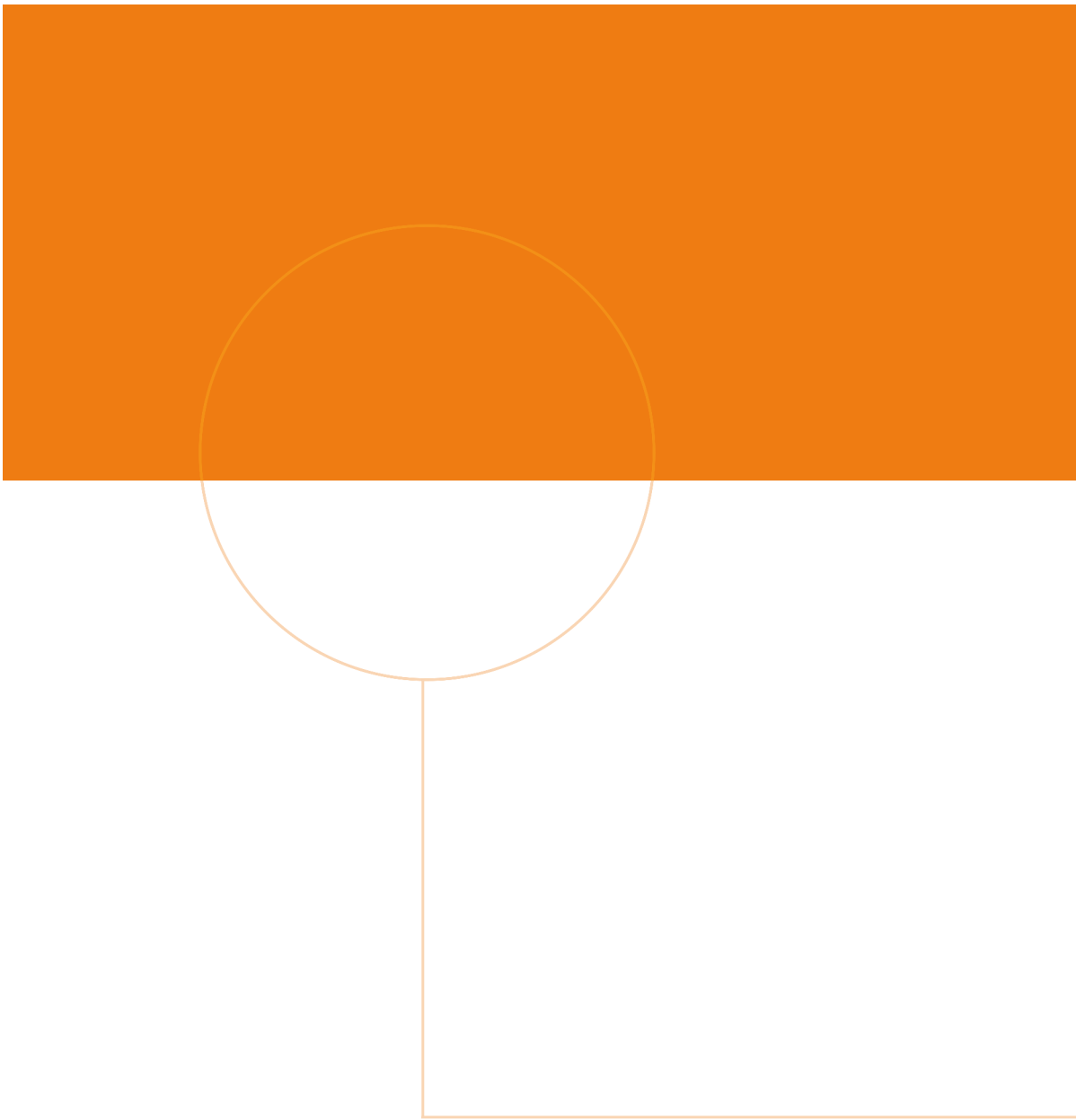

NTNU

Norwegian University of
Science and Technology